LETTER

doi:10.1038/nature13110

Metabolic determinants of cancer cell sensitivity to glucose limitation and biguanides

Kıvanç Birsoy[1,2,3,4]*, Richard Possemato[1,2,3,4]*, Franziska K. Lorbeer[1], Erol C. Bayraktar[1], Prathapan Thiru[1], Burcu Yucel[1], Tim Wang[1,2,3,4], Walter W. Chen[1,2,3,4], Clary B. Clish[3] & David M. Sabatini[1,2,3,4]

As the concentrations of highly consumed nutrients, particularly glucose, are generally lower in tumours than in normal tissues[1,2], cancer cells must adapt their metabolism to the tumour microenvironment. A better understanding of these adaptations might reveal cancer cell liabilities that can be exploited for therapeutic benefit. Here we developed a continuous-flow culture apparatus (Nutrostat) for maintaining proliferating cells in low-nutrient media for long periods of time, and used it to undertake competitive proliferation assays on a pooled collection of barcoded cancer cell lines cultured in low-glucose conditions. Sensitivity to low glucose varies amongst cell lines, and an RNA interference (RNAi) screen pinpointed mitochondrial oxidative phosphorylation (OXPHOS) as the major pathway required for optimal proliferation in low glucose. We found that cell lines most sensitive to low glucose are defective in the OXPHOS upregulation that is normally caused by glucose limitation as a result of either mitochondrial DNA (mtDNA) mutations in complex I genes or impaired glucose utilization. These defects predict sensitivity to biguanides, antidiabetic drugs that inhibit OXPHOS[3,4], when cancer cells are grown in low glucose or as tumour xenografts. Notably, the biguanide sensitivity of cancer cells with mtDNA mutations was reversed by ectopic expression of yeast NDI1, a ubiquinone oxidoreductase that allows bypass of complex I function[5]. Thus, we conclude that mtDNA mutations and impaired glucose utilization are potential biomarkers for identifying tumours with increased sensitivity to OXPHOS inhibitors.

As nutrient concentrations in tumours are different to those in normal tissues, cancer cells *in vivo* may have metabolic dependencies that are not shared by normal cells[6]. In particular, tumour glucose concentrations are frequently 3- to 10-fold lower than in non-transformed tissues[1,7], probably as a result of the high rate of glucose consumption by cancer cells and the poor tumour vasculature. To study the metabolic dependencies imposed on cancer cells by a chronically low-glucose environment, we developed a continuous-flow culture system for maintaining proliferating cells in reduced but steady glucose concentrations for long periods of time. In this system, which we call a Nutrostat, media of a defined glucose concentration is fed into a suspension culture while spent media is removed at the same rate (Fig. 1a). By measuring cell proliferation and glucose concentrations, glucose consumption can be predicted and glucose levels in the intake media can be adjusted so that culture glucose concentrations remain within a 0.5-mM window (Fig. 1b). Jurkat leukaemia cells seeded into 1 mM glucose media in a traditional culture vessel rapidly ceased proliferating as glucose became depleted (Extended Data Fig. 2). In contrast, in a Nutrostat maintained at approximately 0.75 mM glucose, Jurkat cells proliferated exponentially at a rate that was only slightly less than in approximately 10 mM glucose (doubling time of 26 versus 24 h, Fig. 1b). Despite having a small effect on Jurkat cell proliferation, long-term culture in low glucose caused profound metabolic changes: rates of glucose consumption, lactate production and ATP levels decreased as did levels of intermediates in the upper glycolysis and pentose-phosphate pathways (Fig. 1c, d).

To determine whether all cancer cells respond similarly to long-term low-glucose culture, we undertook a competitive proliferation assay with a pooled collection of 28 patient-derived cancer cell lines, each marked with a lentivirally transduced DNA barcode (Fig. 2a). All cell lines were capable of proliferating in suspension and many were derived from blood cancers but also from breast, lung, stomach and colon cancers. The relative abundance of each cell line at the initial seeding and after three weeks in culture at 0.75 or 10 mM glucose was determined by

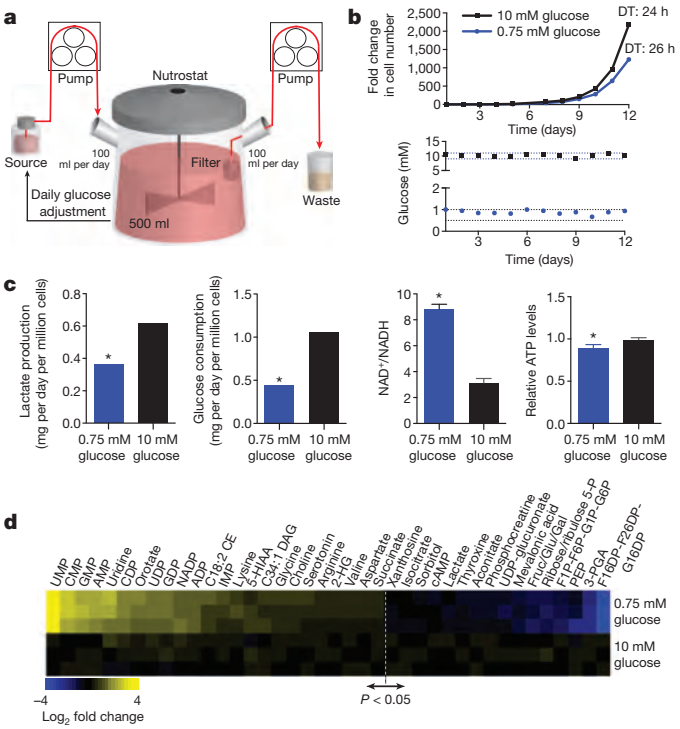

Figure 1 | Nutrostat design and metabolic characterization of cancer cells under chronic glucose limitation. **a**, Nutrostat schematic. **b**, Fold change in cell number (top) and media glucose concentration (bottom) of Jurkat cells grown in Nutrostats at 10 mM (black) or 0.75 mM (blue) glucose. DT, doubling time. **c**, Indicated metabolite levels in Nutrostats at 10 mM (black) or 0.75 mM (blue) glucose. **d**, Differential intracellular metabolite abundances ($P < 0.05$) from cells in Nutrostats at 10 mM (bottom three rows) or 0.75 mM (top three rows) glucose, relative to the average abundance in 10 mM glucose. Colour bar indicates scale (Log_2 transformed). Error bars are s.e.m. ($n = 2$ (glucose and lactate), 3 (NAD(H) ratio) and 8 for ATP levels). Replicates are biological, means reported. *$P < 0.05$ by two-sided Student's *t*-test. C18:2 and C34:1, the number of carbons and number of unsaturated linkages (separated by colons).

[1]Whitehead Institute for Biomedical Research, Nine Cambridge Center, Cambridge, Massachusetts 02142, USA. [2]Howard Hughes Medical Institute and Department of Biology, Massachusetts Institute of Technology, Cambridge, Massachusetts 02139, USA. [3]Broad Institute of Harvard and MIT, Seven Cambridge Center, Cambridge, Massachusetts 02142, USA. [4]The David H. Koch Institute for Integrative Cancer Research at MIT, 77 Massachusetts Avenue, Cambridge, Massachusetts 02139, USA.
*These authors contributed equally to this work.

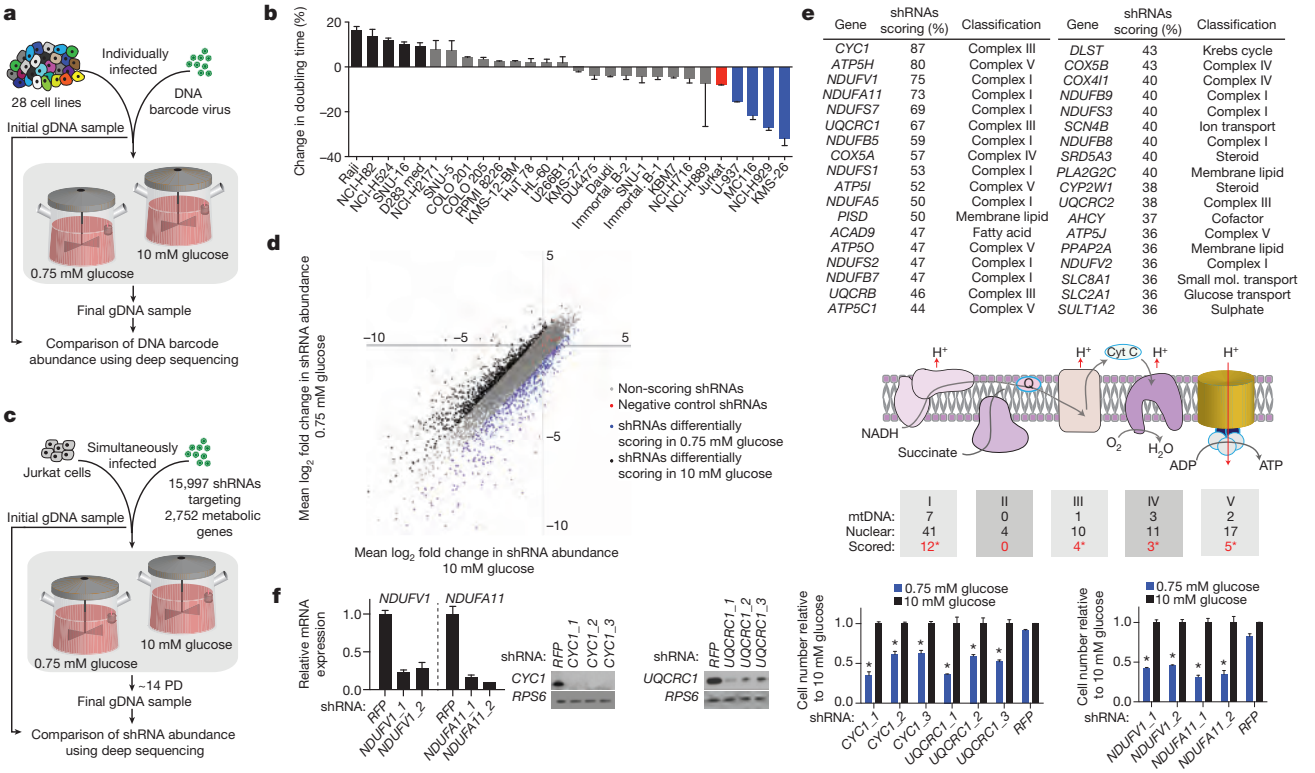

Figure 2 | Barcode-based cell competition assay and RNAi screen in Nutrostats. **a**, Experimental design of cell competition assay. gDNA, genomic DNA. **b**, Per cent changes in doubling times of indicated cell lines in the competition assay, benchmarked to Jurkat cells (red), relative to 0.75 mM glucose. Significant increase (black) or decrease (blue) in doubling time indicated ($P < 0.05$). **c**, Experimental design outline of RNAi-based screen. PD, population doubling. **d**, Primary screening data (mean $\log_2$ fold change) in 10 mM (*x* axis) versus 0.75 mM (*y* axis) glucose. **e**, Genes scoring as preferentially required in 0.75 mM glucose (top); diagram of mitochondrial OXPHOS Complexes (middle); and the number of mitochondria- or nuclear-encoded components and number of nuclear-encoded genes that scored in **e** are indicated (bottom, red). *P* values were obtained by chi-squared tests for complex I ($^*P < 9.3 \times 10^{-49}$), III ($^*P < 6.6 \times 10^{-20}$), IV ($P < 8.3 \times 10^{-10}$) and V ($P < 5.6 \times 10^{-19}$). Q, ubiquinone. **f**, Gene suppression of cells expressing indicated shRNAs (left) and proliferation (right) in 0.75 mM (blue) relative to 10 mM glucose (black). $^*P < 0.05$ relative to control shRNA (shRFP) by two-sided Student's *t*-test, 0.75 mM glucose. Error bars are s.e.m. ($n = 3$). Replicates are biological, means reported.

deep sequencing of the barcodes, and the change in doubling time calculated for each cell line (Fig. 2b and Supplementary Table 1). Interestingly, cancer cell lines exhibit diverse responses to glucose limitation, as the proliferation of many was unaffected, whereas that of a subset was strongly reduced and another, unexpectedly, increased (Fig. 2b). The presence or absence of known oncogenic mutations did not correlate with differences in low-glucose sensitivity.

To understand the metabolic processes that mediate the response to glucose limitation, we used a cell line of modest glucose sensitivity (Jurkat) to undertake a pooled RNAi screen of 2,752 human metabolic enzymes and small molecule transporters (15,997 total short hairpin RNAs (shRNAs); 5 to 10 shRNAs per gene) in high- or low-glucose media in Nutrostats (Fig. 2c). For control shRNAs and the great majority of gene-targeting shRNAs, the average fold change in shRNA abundance was similar in both conditions (Fig. 2d and Supplementary Table 2). However, 10.5% of shRNAs were differentially depleted and, based on our hit criteria (see Methods; for alternative criteria[8] see Supplementary Table 3), we identified 28 and 36 genes whose suppression preferentially inhibited cell proliferation in high or low glucose, respectively (Fig. 2e and Extended Data Fig. 3a). Genes selectively required in 10 mM glucose fell into several pathways but were enriched for glycolytic genes (*GAPDH*, *ALDOA*, *PKM*, *ENO1*; $P < 8.6 \times 10^{-7}$). In marked contrast, genes selectively required under 0.75 mM glucose consisted almost exclusively of the nuclear-encoded components of mitochondrial OXPHOS (Fig. 2e). Among the scoring genes were six of the seven nuclear-encoded core complex I subunits conserved between mammals and bacteria[9], a significant enrichment compared to non-core subunits ($P < 0.0012$, Extended Data Fig. 3b). Two genes required for OXPHOS function, *ACAD9* and *PISD*[9,10], also scored, as did *SLC2A1*, the gene encoding the GLUT1 glucose transporter. Short-term individual assays validated that efficient suppression of top scoring OXPHOS genes selectively decreased proliferation under low glucose, whereas hairpins targeting non-scoring OXPHOS genes did so to a significantly lesser extent (Fig. 2f and Extended Data Fig. 3c). Thus, a screen of metabolic genes pinpointed OXPHOS as the key metabolic process required for optimal proliferation of cancer cells under glucose limitation.

Given these very clear results it seemed likely that fundamental differences in mitochondrial function exist between cancer cell lines that are most sensitive (U-937, MC116, NCI-H929, KMS-26) and resistant (Raji, NCI-H82, NCI-H524, SNU-16, NCI-H2171) to glucose limitation. However, we did not detect any differences in mtDNA content, mitochondrial mass, and baseline oxygen consumption rate (OCR, Extended Data Fig. 4a, b). Therefore, we considered whether a key difference is in the mitochondrial response to glucose limitation, which reversibly induces oxygen consumption[11] (Extended Data Fig. 4c). Indeed, when cultured in low-glucose media, the low-glucose-sensitive cell lines upregulated OCR less than the resistant ones (Fig. 3a). Furthermore, in response to the mitochondrial uncoupling agent FCCP (carbonyl cyanide p-trifluoromethoxyphenylhydrazone), low-glucose-sensitive cell lines induced OCR to a lesser extent than resistant lines, indicating they have reduced spare respiratory capacities (Fig. 3b).

We considered two explanations for why low-glucose-sensitive lines do not substantially increase oxygen consumption upon glucose limitation: first, a defect in glucose utilization that limits substrates for mitochondria; or second, a defect in OXPHOS itself. Consistent with the first possibility, glucose consumption (Fig. 3c) and import (Extended Data

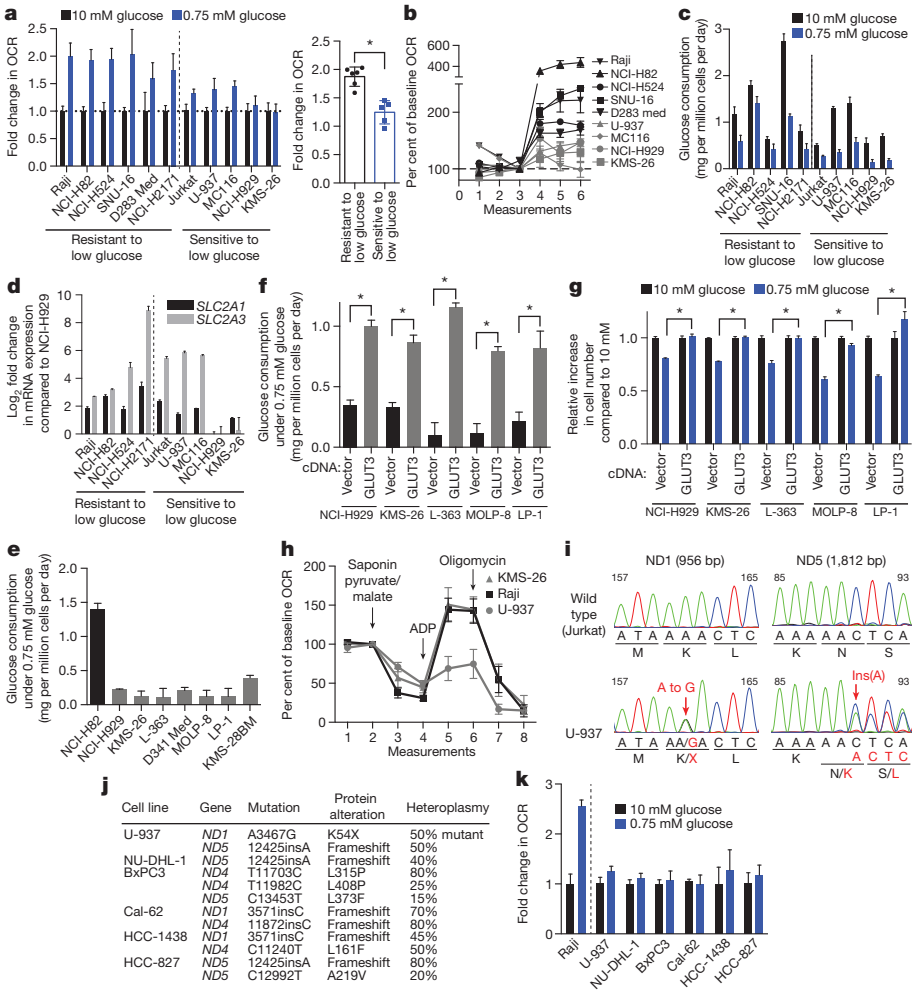

Cell line	Gene	Mutation	Protein alteration	Heteroplasmy
U-937	*ND1*	A3467G	K54X	50% mutant
	ND5	12425insA	Frameshift	50%
NU-DHL-1	*ND5*	12425insA	Frameshift	40%
BxPC3	*ND4*	T11703C	L315P	80%
	ND4	T11982C	L408P	25%
	ND5	C13453T	L373F	15%
Cal-62	*ND1*	3571insC	Frameshift	70%
	ND4	11872insC	Frameshift	80%
HCC-1438	*ND1*	3571insC	Frameshift	45%
	ND4	C11240T	L161F	50%
HCC-827	*ND5*	12425insA	Frameshift	80%
	ND5	C12992T	A219V	20%

Figure 3 | Deficiencies in glucose utilization or complex I underlie low-glucose sensitivity of cancer cells. **a**, Fold change in oxygen consumption rate (OCR) in 0.75 (blue) relative to 10 mM glucose (black) in indicated cell lines individually (left) or in aggregate (right). **b**, Per cent of baseline OCR relative to third measurement and after addition of FCCP (measurements 4–6) in low-glucose-resistant (black) or low-glucose-sensitive (grey) cell lines. **c**, Glucose consumption rate in 10 mM (black) or 0.75 mM glucose (blue). **d**, Expression (qPCR) of *SLC2A1* (black) or *SLC2A3* (grey) in indicated cell lines ($\log_2$ scale relative to NCI-H929). **e**, **f**, Glucose consumption rate of indicated cell lines under 0.75 mM glucose. **g**, Proliferation (4 days) of control (Vector) or GLUT3 overexpressing (GLUT3) cell lines in 10 mM (black) or 0.75 mM glucose (blue). **h**, Per cent of baseline OCR relative to second measurement of saponin-permeabilized lines given indicated substrates. **i**, Sanger sequencing of *ND1* and *ND5* with corresponding wild-type (black) and mutant (red) nucleotide and protein sequences. **j**, mtDNA mutations in complex I genes identified in indicated cell lines. **k**, Fold increase in OCR of indicated cell lines in 0.75 mM (blue) relative to 10 mM glucose (black). Error bars are s.e.m. $n = 6$ for **a**, **b**, **h**, **k**; $n = 5$ for **c**, **e**, **f**; $n = 3$ for **d**, **g**. Replicates are biological, means reported. $^*P < 0.05$ by two-sided student's *t*-test.

Fig. 4d) under low-glucose conditions were defective in two (NCI-H929 and KMS-26) of the low-glucose-sensitive cell lines. Analysis of publicly available gene expression data revealed that these cell lines have low expression of the GLUT3 and GLUT1 glucose transporters, which we verified by quantitative PCR (qPCR) (Fig. 3d), as well as lower levels of several glycolytic enzymes (Extended Data Fig. 4e). Using gene expression data for 967 cell lines[12] we identified additional lines with this expression signature and obtained five of them (Extended Data Fig. 5 and Supplementary Table 4). In low-glucose media, the five lines (LP-1, L-363, MOLP-8, D341 Med, KMS-28BM) had the predicted defect in glucose consumption and proliferation, like NCI-H929 and KMS-26 cells (Fig. 3e and Extended Data Fig. 8b). In all cell lines tested (KMS-26, NCI-H929, L-363, LP-1, MOLP-8), GLUT3 overexpression was sufficient to rescue these phenotypes (Fig. 3f, g, and Extended Data Fig. 4f), without substantially affecting proliferation in high glucose (Extended Data Fig. 4g), arguing that a glucose utilization defect can account for why the proliferation of certain cancer cells is sensitive to low glucose. Indeed, in a competitive proliferation assay, overexpression of GLUT3 provides a growth advantage to KMS-26 cells compared to vector infected controls grown under 0.75 to 2.0 mM glucose in culture and in tumour xenografts (Extended Data Fig. 6).

To investigate whether defects in OXPHOS may be a distinct mechanism underlying low-glucose sensitivity, we focused on U-937 cells as they have low basal OCR but normal glucose utilization (Fig. 3c and Extended Data Fig. 4a). Indeed, in permeabilized-cell mitochondrial-function assays, U-937 cells had a profound defect in using substrates for complexes I (pyruvate and malate) and II (succinate), but not complex IV (TMPD (tetramethylphenylenediamine) and ascorbate) (Fig. 3h and Extended Data Fig. 4h). Sequencing of the seven complex I subunits encoded by the mitochondrial genome (mtDNA) revealed heteroplasmic truncating mutations in *ND1* and *ND5* in U-937 cells (Fig. 3i).

We used available cancer genome resequencing data and information from the literature[12,13] to identify additional cell lines with mtDNA mutations in complex I subunits and obtained five, including two with the same ND5 mutation as U-937 cells (Fig. 3j and Extended Data Fig. 7). Like U-937, the additional lines (BxPC3, Cal-62, HCC-1438, HCC-827, NU-DHL-1) weakly boosted OCR in low-glucose media (Fig. 3k) and had a proliferation defect in this condition (Extended Data Fig. 8b). To investigate whether these phenotypes are caused by complex I dysfunction, we expressed the *Saccharomyces cerevisiae NDI1* gene, which catalyses electron transfer from NADH to ubiquinone without proton translocation[5,14]. NDI1 expression significantly increased the basal OCR of the complex I defective cells (Cal-62, HCC-827, BxPC3, U-937) and partly rescued their proliferation defect in low glucose, but did not substantially affect proliferation in high glucose (Extended Data Fig. 4f, i–l). In an alternative approach, culture of Cal-62 cells for 1.5 months in the presence of a complex I inhibitor (phenformin) produced a population of cells with significantly enriched wild-type mtDNA content and a corresponding decrease in sensitivity to low glucose, changes not observed in cells expressing NDI1 (Extended Data Fig. 9). Taken together, these data identify defective glucose utilization and mitochondrial dysfunction as two distinct mechanisms for conferring sensitivity to glucose limitation on cancer cell lines.

RNAi-mediated suppression of OXPHOS exacerbated the modest sensitivity of Jurkat cells to low glucose (Fig. 2). Thus, we wondered whether low-glucose-sensitive cells lines may be, like LKB1-deficient cells[15], particularly sensitive to the biguanide class of pharmacological OXPHOS inhibitors[3,4] that includes metformin and the more potent biguanide

phenformin[3]. Indeed, in low-glucose media, cell lines with mtDNA-encoded complex I mutations (U-937, BxPC3, Cal-62, HCC-1438, HCC-827, NU-DHL-1) or impaired glucose utilization (NCI-H929, KMS-26, LP-1, L-363, MOLP-8, D341 Med, KMS-28BM) were 5- to 20-fold more sensitive to phenformin compared to control cancer cell lines or an immortalized B-cell line (Fig. 4a), and similar results were obtained with metformin or when using direct cell counting as a readout (Extended Data Fig. 8a, b, d). The low-glucose-sensitive cell lines, particularly those with impaired glucose utilization, tended to be more sensitive to phenformin in 0.75 than 10 mM glucose, but substantial sensitivity persisted at 1.5 to 3.0 mM glucose (Fig. 4b and Extended Data Fig. 8c, e). Importantly, in cells with impaired glucose utilization, GLUT3 overexpression almost completely rescued the phenformin sensitivity specific to the low-glucose condition, such that GLUT3-expressing cells in 0.75 mM glucose and control cells in 10 mM glucose were similarly affected by phenformin (Fig. 4c). Likewise, in cells with mutations in complex I, NDI1 expression almost completely rescued the effects of phenformin on proliferation (Fig. 4d) and oxygen consumption (Fig. 4e and Extended Data Fig. 8g). Phenformin sensitivity is restricted to cells with the intermediate levels of mitochondrial dysfunction typically seen in cancer cells, as cells lacking mtDNA (143B Rho) are insensitive to phenformin but sensitive to low glucose (Extended Data Fig. 8h).

Consistent with these findings and with the low-glucose environment of tumours[1,2,7], phenformin inhibited the growth of mouse tumour xenografts derived from cancer cells with mtDNA mutations (Cal-62, U-937) or poor glucose consumption (KMS-26, NCI-H929), but not from cells lacking these defects (NCI-H2171 and NCI-H82) (Fig. 4f, g). The effects of phenformin on tumour xenograft growth were rescued in mtDNA mutant cells by the introduction of NDI1, and in KMS-26 cells by the overexpression of GLUT3 (Fig. 4g and Extended Data Fig. 8f), demonstrating that the effect of phenformin on these xenografts has a cell-autonomous component. Thus, the glucose-utilization gene signature described earlier and mutations in mtDNA-encoded complex I subunits may serve as biomarkers for identifying tumours that are particularly sensitive to phenformin treatment. Such tumours are probably relatively common, as the prevalence of truncating mutations in mtDNA-encoded OXPHOS components is reported to be as high as 16%[16] and we detect the low-glucose-import gene expression signature in at least 5% of cell lines profiled (of which multiple myeloma and small cell lung cancer are significantly enriched). Interestingly, a number of

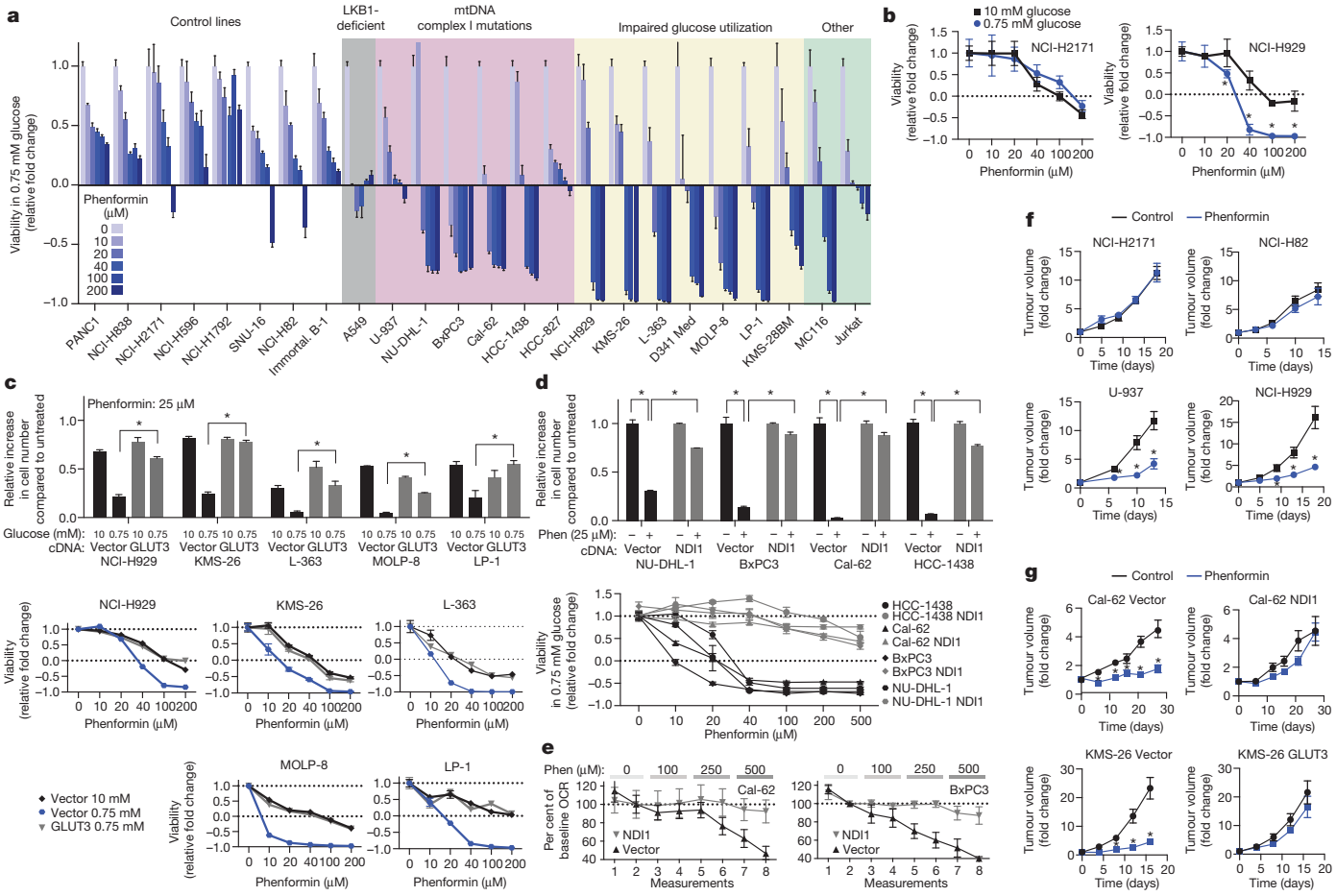

Figure 4 | Cancer cells with deficiencies in glucose utilization or complex I are sensitive to phenformin. **a**, Viability of indicated lines, as measured by ATP levels on day 3 at phenformin concentrations indicated by black–blue scale, in 0.75 mM glucose, compared to ATP levels on day 0. Value of 1 indicates fully viable cells (untreated). Value of 0 indicates no change in ATP level compared to day 0 (cytostatic). Negative values indicate decrease in ATP levels (−1 indicates no ATP). **b**, Viability as in **a** of NCI-H2171 and NCI-H929 cell lines under 0.75 and 10 mM glucose. **c**, Relative increase in cell number (top) and viability as in **a** (bottom) of control (Vector) or GLUT3 overexpressing (GLUT3) cell lines in 10 mM or 0.75 mM glucose at indicated phenformin concentrations relative to untreated cells in 10 mM glucose. **d**, Relative increase in cell number (top) and viability as in **a** (bottom) of vector control (black) or NDI1 (grey) expressing lines in 0.75 mM glucose at indicated phenformin concentrations relative to untreated cells in 0.75 mM glucose. **e**, Per cent of baseline OCR relative to second measurement of control (Vector) or NDI1-expressing lines (NDI1) relative to the second basal measurement at indicated phenformin concentrations. **f**, Average volume (relative to day 0) of established xenografted tumours derived from control (NCI-H2171, NCI-H82), mtDNA complex I mutant (U-937), or impaired glucose utilization (NCI-H929) cell lines in mice treated with vehicle (black) or phenformin (blue) in drinking water starting at day 0. **g**, Average tumour volume as in **f** of indicated cell lines infected with control, NDI1- or GLUT3-expressing vectors. Error bars are s.e.m. $n = 5$ for **a**, **b**, **c** (bottom), **d** (bottom), **e**, **f**; $n = 6$ (control) or $n = 8$ (GLUT3 or NDI1) for **g**; $n = 3$ for **c** (top), **d** (top). Replicates are biological, means reported. $^*P < 0.05$ by two-sided student's t-test.

retrospective studies report survival benefits for cancer patients taking metformin[17,18], although it has been unclear whether these effects of metformin are cancer cell-autonomous[15,19,20].

In conclusion, we find that cancer cells exhibit diverse responses to glucose limitation and identify defects in glucose utilization and mitochondrial function as major determinants of low-glucose sensitivity (Extended Data Fig. 1). These biomarkers may pinpoint cancer cells that are likely to respond to OXPHOS inhibition alone under tumour-relevant glucose concentrations. Such a targeted strategy may be better tolerated than previously proposed approaches of combining inhibition of OXPHOS and glycolysis[21–23]. Moreover, our findings underscore the importance of considering glucose concentrations when evaluating the sensitivity of cancer cells to biguanides or other OXPHOS inhibitors. The methods described here should be valuable for studying the responses of cancer cells to tumour-relevant concentrations of other highly consumed nutrients, such as amino acids[24], and to additional compounds that target metabolism.

METHODS SUMMARY

Glucose concentrations were maintained in Nutrostats by continuous flow of fresh media at defined glucose concentrations and simultaneous removal of spent media at a fixed rate. Competition assays were carried out at 10 or 0.75 mM glucose in Nutrostats using cell lines barcoded with lentivirally transduced seven-base-pair sequences. Nutrostats were used under similar conditions for the pooled RNAi screen of 2,752 metabolic genes and metabolite transporters. Barcode or shRNA abundances in cells were determined using deep sequencing and compared to initial cultures. Genome resequencing data were used to identify cancer cell lines with mitochondrial genome mutations and the Seahorse Extracellular Flux Analyzer was used to assay mitochondrial function. Defects in glucose import were identified using expression analyses of genes encoding glucose transporters and glycolytic enyzmes.

Online Content Any additional Methods, Extended Data display items and Source Data are available in the online version of the paper; references unique to these sections appear only in the online paper.

Received 8 August 2013; accepted 29 January 2014.
Published online 16 March 2014.

1. Hirayama, A. *et al.* Quantitative metabolome profiling of colon and stomach cancer microenvironment by capillary electrophoresis time-of-flight mass spectrometry. *Cancer Res.* **69,** 4918–4925 (2009).
2. Gullino, P. M., Grantham, F. H. & Courtney, A. H. Glucose consumption by transplanted tumors *in vivo*. *Cancer Res.* **27,** 1031–1040 (1967).
3. Owen, M. R., Doran, E. & Halestrap, A. P. Evidence that metformin exerts its anti-diabetic effects through inhibition of complex 1 of the mitochondrial respiratory chain. *Biochem. J.* **348,** 607–614 (2000).
4. El-Mir, M. Y. *et al.* Dimethylbiguanide inhibits cell respiration via an indirect effect targeted on the respiratory chain complex I. *J. Biol. Chem.* **275,** 223–228 (2000).
5. Seo, B. B., Matsuno-Yagi, A. & Yagi, T. Modulation of oxidative phosphorylation of human kidney 293 cells by transfection with the internal rotenone-insensitive NADH-quinone oxidoreductase (NDI1) gene of *Saccharomyces cerevisiae*. *Biochim. Biophys. Acta* **1412,** 56–65 (1999).
6. Cairns, R. A., Harris, I. S. & Mak, T. W. Regulation of cancer cell metabolism. *Nature Rev. Cancer* **11,** 85–95 (2011).
7. Urasaki, Y., Heath, L. & Xu, C. W. Coupling of glucose deprivation with impaired histone H2B monoubiquitination in tumors. *PLoS ONE* **7,** e36775 (2012).
8. Luo, B. *et al.* Highly parallel identification of essential genes in cancer cells. *Proc. Natl Acad. Sci. USA* **105,** 20380–20385 (2008).
9. Tasseva, G. *et al.* Phosphatidylethanolamine deficiency in Mammalian mitochondria impairs oxidative phosphorylation and alters mitochondrial morphology. *J. Biol. Chem.* **288,** 4158–4173 (2013).
10. Haack, T. B. *et al.* Exome sequencing identifies ACAD9 mutations as a cause of complex I deficiency. *Nature Genet.* **42,** 1131–1134 (2010).
11. Crabtree, H. G. Observations on the carbohydrate metabolism of tumours. *Biochem. J.* **23,** 536–545 (1929).
12. Barretina, J. *et al.* The Cancer Cell Line Encyclopedia enables predictive modelling of anticancer drug sensitivity. *Nature* **483,** 603–607 (2012).
13. Jones, J. B. *et al.* Detection of mitochondrial DNA mutations in pancreatic cancer offers a ''mass''-ive advantage over detection of nuclear DNA mutations. *Cancer Res.* **61,** 1299–1304 (2001).
14. Santidrian, A. F. *et al.* Mitochondrial complex I activity and NAD^+/NADH balance regulate breast cancer progression. *J. Clin. Invest.* **123,** 1068–1081 (2013).
15. Shackelford, D. B. *et al.* LKB1 inactivation dictates therapeutic response of non-small cell lung cancer to the metabolism drug phenformin. *Cancer Cell* **23,** 143–158 (2013).
16. Larman, T. C. *et al.* Spectrum of somatic mitochondrial mutations in five cancers. *Proc. Natl Acad. Sci. USA* **109,** 14087–14091 (2012).
17. Evans, J. M., Donnelly, L. A., Emslie-Smith, A. M., Alessi, D. R. & Morris, A. D. Metformin and reduced risk of cancer in diabetic patients. *Br. Med. J.* **330,** 1304–1305 (2005).
18. DeCensi, A. *et al.* Metformin and cancer risk in diabetic patients: a systematic review and meta-analysis. *Cancer Prev. Res. (Phila.)* **3,** 1451–1461 (2010).
19. Birsoy, K., Sabatini, D. M. & Possemato, R. Untuning the tumor metabolic machine: targeting cancer metabolism: a bedside lesson. *Nature Med.* **18,** 1022–1023 (2012).
20. Pollak, M. Metformin and pancreatic cancer: a clue requiring investigation. *Clin. Cancer Res.* **18,** 2723–2725 (2012).
21. Hall, A. *et al.* Dysfunctional oxidative phosphorylation makes malignant melanoma cells addicted to glycolysis driven by the (V600E)BRAF oncogene. *Oncotarget* **4,** 584–599 (2013).
22. Ben Sahra, I., Tanti, J. F. & Bost, F. The combination of metformin and 2 deoxyglucose inhibits autophagy and induces AMPK-dependent apoptosis in prostate cancer cells. *Autophagy* **6,** 670–671 (2010).
23. Javeshghani, S. *et al.* Carbon source and myc expression influence the antiproliferative actions of metformin. *Cancer Res.* **72,** 6257–6267 (2012).
24. Jain, M. *et al.* Metabolite profiling identifies a key role for glycine in rapid cancer cell proliferation. *Science* **336,** 1040–1044 (2012).

Supplementary Information is available in the online version of the paper.

Acknowledgements We thank G. Stephanopoulos for assistance with Nutrostat design, M. Holland for mtDNA sequencing consultation, L. Garraway for assistance identifying mtDNA mutant cell lines, T. Yagi for the NDI1 antibody, T. DiCesare for diagrams, and members of the Sabatini Laboratory for assistance (particularly A. Saucedo, C. Koch, O. Yilmaz, Y. Gultekin and A. Hutchins for technical assistance, and D. Lamming and W. Comb for critical reading of the manuscript). This research is supported by fellowships from The Leukemia and Lymphoma Society and The Jane Coffin Childs Fund to K.B., the Council of Higher Education Turkey and Karadeniz T. University Scholarships to B.Y. and grants from the David H. Koch Institute for Integrative Cancer Research at MIT, The Alexander and Margaret Stewart Trust Fund, the NIH (K99 CA168940 to R.P. and CA103866, CA129105, and AI07389 to D.M.S.) and the Starr Cancer Consortium. D.M.S. is an investigator of the Howard Hughes Medical Institute.

Author Contributions K.B., R.P. and D.M.S. conceived the project and designed the experiments. K.B. and R.P. designed and engineered the Nutrostat and performed the screening, knockdown, cell proliferation, extracellular flux, glucose consumption, and tumour formation experiments and processed and analysed sequencing and expression data. F.K.L., E.C.B., B.Y., and W.W.C. assisted with experiments. C.B.C. performed the metabolite profiling experiments. T.W. provided bioinformatic support for shRNA abundance deconvolution, P.T. assisted in identifying mtDNA mutations. K.B., R.L.P and D.M.S. wrote and all authors edited the manuscript.

Author Information Reprints and permissions information is available at www.nature.com/reprints. Readers are welcome to comment on the online version of the paper. The authors declare no competing financial interests. Correspondence and requests for materials should be addressed to D.M.S. (sabatini@wi.mit.edu).

METHODS

The following abbreviations appear in Fig. 1d: 2-HG, 2-hydroxyglutarate; 5-HIAA, 5-hydroxyindoleacetic acid; ADP, adenosine diphosphate; AMP, adenosine monophosphate; cAMP, cyclic AMP; CDP, cytidine diphosphate; CMP, cytidine monophosphate; CE, ceramide; DAG, diacylglycerol (fatty acids additionally have annotations indicating the number of carbons and number of unsaturated linkages separated by a colon (for example, 18:2)); F1P, fructose 1-phosphate; F16DP, fructose 1,6-diphosphate; F26DP, fructose 2,6-diphosphate; F6P, fructose 6-phosphate; FCCP, carbonyl cyanide 4-(trifluoromethoxy)phenylhydrazone; fruc, fluctose; G1P, glucose 1-phosphate; G16DP, glucose 1,6-diphosphate; G6P, glucose 6-phosphate; GDP, guanosine diphosphate; Gal, galactose; Glu, glucose; GMP, guanosine monophosphate; IMP, inosine monophosphate; Mal, malate; NAD^+/NADH, nicotinamide adenine dinucleotide (oxidized and reduced forms); NADP, nicotinamide adenine dinucleotide phosphate; PEP, phosphoenolpyruvate; 3-PGA, 3-phosphoglycerate; Py, pyruvate; TMPD, N,N,N′,N′-tetramethyl-p-phenylenediamine; UDP, uridine diphosphate; UMP, uridine monophosphate.

Cell lines and reagents. Cell lines were obtained from the Broad Institute Cancer Cell Line Encyclopedia with the exceptions of HL-60, Daudi, HuT 78, MC116, Raji and U-937, which were kindly provided by R. Weinberg, KMS-26 and KMS-27, which were purchased from the JCRB Cell Bank, Immortalized B lines 1 and 2, which were provided by C. Klein, and Cal-62, which was provided by J. A. Fagin. To normalize for media-specific effects on cell metabolism, all cell lines were grown in RPMI base medium containing 10% heat inactivated fetal bovine serum, 2 mM glutamine, penicillin and streptomycin. The NDI1 antibody is a kind gift of T. Yagi. Additional antibodies used are: Actin (I-19, Santa Cruz), Glut3 (ab15311, Abcam), RPS6 (Cell Signaling), CYC1 (Sigma) and UQCRC1 (H00007384-B01P, Novus).

Cell lines are from the following cancer origins: PANC1 (pancreas), NCI-H838 (lung), NCI-H596 (lung), NCI-H1792 (lung), A549 (lung), NU-DHL-1 (lymphoma), BxPC3 (pancreas), Cal-62 (thyroid), HCC-1438 (lung), HCC-827 (lung), L-363 (plasma cell leukaemia), MOLP-8 (multiple myeloma), LP-1 (multiple myeloma). Additional cell lines and their tissue origins are listed in Supplementary Table 1. One cell line (SNU-1) was randomly selected for authentication by short tandem repeat (STR) profiling, and cell lines were authenticated by mtDNA sequencing (NCI-H82, Jurkat, NU-DHL-1, U-937, BxPC3, Cal-62, HCC-1438, HCC-827, Raji, MC116, KMS-26, NCI-H929, NCI-H2171).

Lentiviral shRNAs were obtained from The RNAi Consortium (TRC; http://www.broadinstitute.org/rnai/trc/lib) collection of the Broad Institute. The TRC numbers for the shRNAs used are below. For each gene, the order of the TRC numbers matches the order of the shRNAs as numbered in the manuscript. *CYC1* (TRCN0000064606, TRCN0000064603, TRCN0000064605); *UQCRC1* (TRCN 0000233157, TRCN0000046484, TRCN0000046487); *NDUFA7* (TRCN0000026423, TRCN0000026454); *NDUFB1* (TRCN0000027148, TRCN0000027173); *COX5A* (TRCN0000045961, TRCN0000045960); *UQCRH* (TRCN0000046528, TRCN 0000046530); *UQCRFS1* (TRCN0000046522, TRCN0000046519); *NDUFB10* (TRCN0000026589, TRCN0000026579); *UQCR11* (TRCN0000046465, TRCN 0000046467); *NDUFA11* (TRCN0000221374, TRCN0000221376); *NDUFV1* (TRCN0000221380, TRCN0000221378); *PKM* (TRCN0000037612, TRCN0000 195405); *RFP* (TRCN0000072203).

The retroviral *SLC2A3* vector was generated by cloning into the BamHI and EcoRI sites of the pMXS-ires-blast vector a cDNA insert generated by PCR from a cDNA from Open Biosystems (catalogue number MHS1010-7429646) using the primers below, followed by standard cloning techniques: *SLC2A3* (BamHI) forward, GCATGGATCCACCATGGGCACACAGAAGGTCAC; *SLC2A3* (MfeI) reverse, GCATCAATTGTTAGACATTGGTGGTGGTCTCC.

The retroviral NDI1 vector was generated by cloning into the EcoRI and XhoI sites of the pMXS-ires-blast vector a cDNA insert generated by PCR from a yeast genomic library using the primers below, followed by standard cloning techniques: *Ndi1* (EcoRI) forward, ATGAATTCCATCACATCATCGAATTAC; *Ndi1* (XhoI) reverse, ATCTCGAGAAAAGGGCATGTTAATTTCATCTATAAT.

Nutrostat design. Equipment used in constructing the Nutrostat (Fig. 1, see also Extended Data Fig. 10 for schematic): peristaltic pumps with accompanying tubing (Masterflex, manufacturer no. 77120-42), 500 ml spinner flasks (Corning, product no. 4500-500), 9-position stirplate (Bellco Glass, manufacturer no. 7785-D9005) or LABDISC magnetic stirrer (VWR no. 97056-526), Tygon tubing (Saint Gobain Performance Plastics, manufacturer no. ACJ00004 (outlet, 3/32″ × 5/32″) and ABW00001 (inlet, 1/32″ × 3/32″), Outlet filter (Restek, catalogue no. 25008), vented caps for source and waste containers (Bio Chem Fluidics, catalogue no. 00945T-2F), and outlet tubing check valve (Ark-plas, catalogue no. AP19CV0012SL) to prevent backflow. Spinner flasks were siliconized before each use using Sigmacote (Sigma SL2) according to the manufacturer's method, and autoclaved. The outlet filter was cleaned before use by passing phosphate buffered saline and then 70% ethanol through the filter in both the forward and reverse directions. Plastic tubing was replaced before each experiment and was cut to 50- to 60-cm pieces and threaded through the caps for the source or waste vessel, over the peristaltic pump, and through the caps on the spinner flask. The outlet tubing was cut approximately 5 cm from the spinner flask to allow for the introduction of the check valve and prevent back-flow of medium. Tubing was adjusted to the following heights: source vessel, bottom; spinner flask inlet, 3 cm from cap (above media level); spinner flask outlet + filter, empirically adjusted so that the volume of media in the vessel is maintained at 500 ml; waste vessel, 2 cm from the cap. The entire assembled setup was autoclaved before use. The flow rate of the inlet peristaltic pump was adjusted empirically to 100 ml per day using phosphate buffered saline before the introduction of culture media, and the flow rate of the waste pump was set to safely exceed 100 ml per day to prevent accumulation of medium in the vessel. Some escape of cells from the vessel and accumulation in the waste vessel was unavoidable. Medium was sampled directly from the vessel by pipette. The mass of glucose consumed by the Nutrostat over time was modelled by the following equation:

$$G_{\text{nutrostat}}(t) = \int_0^t N_0 \times Q_{\text{glucose}} \times 2^{\frac{t}{a}} dt$$

where N_0 is the starting cell number, Q_{glucose} is the consumption rate of glucose (g per cell per day), a is the doubling time of the cell line (days), and t is time (days). The values for N_0, Q_{glucose} and a were empirically determined before the start of the experiment. The Nutrostat glucose consumption was calculated in hourly increments and balanced by the amount of glucose leaving or entering the chamber such that $G_{\text{nutrostat}}$ over the 1-h time interval = $([\text{Gluc}]_{\text{source}} \times V_{\text{in}}) - ([\text{Gluc}]_{\text{nutrostat}} \times V_{\text{out}})$ where $[\text{Gluc}]_{\text{nutrostat}}$ is the Nutrostat glucose concentration, $[\text{Gluc}]_{\text{source}}$ is the source media glucose concentration, V_{out} is the volume of media leaving the chamber, and V_{in} is the volume of media entering the chamber ($V_{\text{out}} = V_{\text{in}} = 0.1$ litres per day). The $[\text{Gluc}]_{\text{source}}$ was adjusted daily so that the $[\text{Gluc}]_{\text{nutrostat}}$ predicted by the model remained between the desired glucose concentration boundaries, and adherence of the actual glucose concentration in the Nutrostat to the model was periodically evaluated by measuring the glucose concentration of media samples using a glucose oxidase assay (Fisher Scientific, catalogue no. TR-15221).

Pooled shRNA screening. The 2,752 transporters and metabolic enzymes targeted in this study were identified as described[25] and are listed in Supplementary Table 2. Lentiviral plasmids encoding approximately 15,000 shRNAs targeting these genes (median of 5 shRNAs per gene) as well as 30 non-targeting control shRNAs were obtained and combined to generate a single plasmid pool, the composition of which is described in Supplementary Table 2. Plasmid pools were used to generate lentivirus-containing supernatants and target cell lines were infected in 2 μg ml^{-1} polybrene as described[25]. Specifically, the titre of lentiviral supernatants was determined by infecting targets cells at several concentrations, counting the number of drug resistant infected cells after 3 days of selection. Thirty-million target cells were infected at an multiplicity of infection of approximately 0.5 to ensure that most cells contained only a single viral integrant and ensure proper library complexity. Infected cells were selected with 0.5 μg ml^{-1} puromycin for 3 days. Cells containing shRNA pools were used to inoculate Nutrostats at approximately 15 million cells per 500 ml culture. Glucose concentrations were measured daily and adjusted as described above. Cultures were diluted once to ensure the cell density never exceeded 500,000 cells per ml. Cultures were collected for genomic DNA extraction after approximately 15 population doublings, and samples were processed as described[25] except that two rounds of PCR were used and the primers used to amplify shRNA inserts and perform deep sequencing (Illumina) are as provided below. shRNAs present at fewer than 100 reads in the initial post-infection sample were eliminated from further analysis. Because the lentiviral pool contained shRNA expression vectors pLKO.1 and pLKO.005, to eliminate any backbone-specific amplification bias, the abundance measurements of shRNAs in the pLKO.005 vector were normalized such that the distribution of shRNA abundances in the pLKO.005 vector matched the distribution of shRNA abundances in the pLKO.1 vector in each sample. Individual shRNAs were identified as differentially scoring in high glucose versus low glucose using a $\log_2$ fold change cutoff of −0.75 (high glucose versus low glucose). For each comparison, genes were considered hits if >33% of the shRNAs targeting that gene scored when averaging across all replicates ('Per cent shRNAs scoring' reported in Fig. 2e). Pathways scoring as preferentially required in low glucose are complex I ($P < 9.3 \times 10^{-49}$), III ($P < 6.6 \times 10^{-20}$), IV ($P < 8.3 \times 10^{-10}$) and V ($P < 5.6 \times 10^{-19}$). The 1 or 2 genes from complex I, III and IV that scored most highly according to 'Per cent shRNAs scoring', were chosen for validation and are reported in Fig. 2f (complex I genes *NDUFV1* and *NDUFA11*, and complex III genes *CYC1* and *UQCRC1*) and Extended Data Fig. 3 (complex IV gene *COX5A*). Complex I was studied further in Fig. 3i–k and Fig. 4 using a specific inhibitor (phenformin), as this was the most significantly scoring pathway and because mutations were identified in mitochondrially encoded complex I subunits in several cell lines, and a high prevalence of somatic mutations in mtDNA-encoded complex I genes have been reported previously in human tumours.

The GENE-E program[8] (Broad Institute) was used as an alternative method for identifying hits from RNAi-based screens, and these results are reported in Supplementary Table 3. These alternative methods all identify highly significant numbers of complex I, III, IV and V genes as being differentially essential in 0.75 mM glucose.

Primers for amplifying shRNAs encoded in genomic DNA: first round of PCR (15 cycles), forward, AATGGACTATCATATGCTTACCGTAACTTGAAAGTATTTCG, reverse, CTTTAGTTTGTATGTCTGTTGCTATTATGTCTACTATTCTTTCCC; second round of PCR, barcoded forward primer (N indicates locations of sample-specific barcode sequences), AATGATACGGCGACCACCGAGAAAGTATTTCGATTTCTTGGCTTTATATATCTTGTGGANNNNACGA; common reverse primer, CAAGCAGAAGACGGCATACGAGCTCTTCCGATCTTGTGGATGAATACTGCCATTTGTCTCGAGGTC; Illumina sequencing primer, AGAAAGTATTTCGATTTCTTGGCTTTATATATCTTGTGGA.

Cell barcoding. To mark individual cell lines with DNA barcodes, a unique seven-base-pair sequence was transduced into cells using lentiviruses produced from a pLKO.1P vector into which the following sequence was cloned using the following primers, which had been annealed and ligated to a restriction-enzyme-cut vector (AgeI and EcoRI restriction enzymes): sequence inserted (N indicates locations of cell-specific barcode sequences): TTTTAGCACTGCCNNNNNNNCTCGCGGGCCGCAGGTCCAT; primers, top, CCGGTTTTTAGCATCGCCNNNNNNNCTCGCGGCCGCAGGTCCATG, bottom, AATTCATGGACCTGCGGCCGCGAGNNNNNNNGGCGATGCTAAAAA.

The sequence of individual lentiviral vectors was determined by Sanger sequencing and vectors containing unique sequences were chosen for transduction into cell lines. Each cell line was infected with three barcodes in separate infections so that the proliferation of each cell line could be measured three times independently in a single experiment. Proliferation assays of the individually barcoded cell lines verified that the barcodes did not affect cell proliferation in short term assays. To perform the cell competition assays, all of the barcoded cell lines were mixed in equal proportion with bias for overrepresentation of slower-proliferating cell lines in the initial population. The Nutrostats were inoculated with 5 million pooled cells at 10 mM or 0.75 mM glucose concentrations and the proliferation and glucose consumption of the culture carefully monitored to adjust for any time-dependent changes in the per-cell glucose consumption rate. After 15 population doublings, cells were collected for genomic DNA isolation and processed for deep sequencing as described above. Barcode abundance was determined in the starting population or after 15 population doublings, and the fold change in barcode abundance relative to the abundance of Jurkat cell line barcodes was calculated. Based on the number of population doublings of the entire culture and the known doubling time of the Jurkat cell line, the doubling time (hours) of each cell line in the mixture was calculated according to the following formula:

$$293\ \text{h} / (\log_2 \text{FC}_{\text{cell line}} - \log_2 \text{FC}_{\text{Jurkat}} + \text{PD}_{\text{Jurkat}})$$

where 293 h is the duration of the experiment, $\log_2 \text{FC}_{\text{cell line}}$ is the $\log_2$ fold change in abundance of barcode for the given cell line in the final sample compared to the initial, $\log_2 \text{FC}_{\text{Jurkat}}$ is the $\log_2$ fold change for the Jurkat cell line, and $\text{PD}_{\text{Jurkat}}$ is the empirically determined number of population doublings that the Jurkat cell line underwent during 293 h (that is, 12.2 doublings in 10 mM glucose and 11.3 doublings in 0.75 mM glucose conditions). These calculated doubling times are reported for each barcode replicate in Supplementary Table 1.

Glucose consumption and uptake. Cells were plated in 10 mM or 0.75 mM glucose medium at 5,000 to 20,000 cells per ml in 24-well plates in 1 ml medium in replicates of four. Media were collected after 4 days of culture and the number of cells counted. Harvested media were assayed by a glucose oxidase assay and the absorbance at 500 nm determined of assay buffer plus spent media, media from control wells containing no cells, or media containing no glucose, allowing the concentration of glucose in the spent media to be calculated according to Beer's Law. The mass of glucose consumed was normalized to the average number of cells present in the well, which was calculated by integrating the number of cells present during the course of the experiment over 4 days assuming simple exponential growth of the cells during the course of the experiment from the measured starting to final number of cells. For glucose import, cells were incubated in 0.75 mM glucose medium overnight. The following day, Tritium-labelled 2-DG (5 μCi ml^{-1}, Moravek) in RPMI was added to 300,000 cells in fresh 0.75 mM glucose medium. The import was stopped after 30, 60 and 120 min by the addition of cold HBSS (Hank's balanced salt solution) containing the glucose transporter inhibitor cytochalasin B. The cells were next washed once with ice-cold HBSS and lysed in 400 μl RIPA (radio-immunoprecipitation assay) buffer with 1% SDS. Radioactive counts were determined by a scintillation counter and scintillation reads were normalized to the total protein concentration of each sample.

Metabolite profiling. For metabolite-concentration measurements, 10-million Jurkat cells were cultured in Nutrostats for 2 weeks before metabolite extraction. Cells were rapidly washed three times with cold PBS, and metabolites were extracted by the addition of 80% ice-cold methanol. Endogenous metabolite profiles were obtained using liquid chromatography–mass spectrometry (LC–MS) as described previously[26]. Metabolite levels ($n = 3$ biological replicates) were normalized to cell number.

Lactate and NAD(H) measurements. Lactate was measured as previously described[25] using the same medium that was used for glucose consumption measurements (above). NAD(H) was measured using the Fluoro NAD kit (Cell Technology FLNADH 100-2) in accordance with the manufacturer's protocol.

Bioinformatic identification of cell lines with impaired glucose utilization. Gene expression data for all glycolytic genes and glucose transporters were compared between glucose-utilization-deficient cell lines (KMS-26 and NCI-H929) and all of the other cell lines, and those genes whose expression was significantly lower in the glucose-utilization-deficient lines were selected (*SLC2A1*, *HK1*, *GAPDH*, *ENO1*, *GPI*, *TPI1* and *PKM*). *SLC2A3* was also included as its expression was found to be significantly altered using qPCR (Fig. 3d). Log_2-transformed expression data for these eight genes was extracted for all 967 cell lines from the Cancer Cell Line Encyclopedia. For each cell line, we computed the difference between the expression level of each gene and the median expression level in all cell lines. For each gene, the cell lines were ranked in order of gene expression from lowest to highest, and these ranks were summed across all eight genes. (Supplementary Table 4). Those cell lines included KMS-26 and NCI-H929, and from the other 30 cell lines with the lowest expression level of these genes, readily available lines were chosen.

Identification of cell lines with mutations in mtDNA-encoded complex I subunits. Hybrid capture genome resequencing data of 912 cell lines from the Broad Institute Cancer Cell Line Encyclopedia (data kindly provided by L. Garraway) were mined for spurious mtDNA reads, which were aligned to the Revised Cambridge Reference Sequence. Sufficient data were obtained to reach an average of 5× coverage in 504 cell lines. Cell lines with frameshifting insertions or deletions in complex I subunits were identified from the data, and the presence of the predicted mutations confirmed by Sanger sequencing using the primers listed below in PCR followed by sequencing reactions. The degree of heteroplasmy was estimated based upon the ratio of the area under the curves of the wild-type allele to the mutant allele from Sanger sequence traces. Common variants were identified and filtered out by comparison to a database of such variants (MITOMAP: http://www.mitomap.org) and by the presence of these variants in >1% of the other cell lines in the CCLE set.

Primers for sequencing of mtDNA-encoded complex I genes: *ND1*, *MT-ND1* forward, GGTTTGTTAAGATGGCAGAGCCC, *MT-ND1* reverse, GATGGGTTCGATTCTCATAGTCCTAG; *ND2*, *MT-ND2* forward, TAAGGTCAGCTAAATAAGCTATCGGGC, *MT-ND2* reverse, CTTAGCTGTTACAGAAATTAAGTATTGCAAC; *ND3*, *ND4L* and 5′ end of *ND4*, *MT-ND3* and *MT-ND4* forward, TTGATGAGGGTCTTACTCTTTTAGTATAAAT; *MT-ND3* and *MT-ND4* reverse, GATAAGTGGCGTTGGCTTGCCAT; 3′ end of *ND4*, *MT-ND4* forward, CCTTTTCCTCCGACCCCCTAACA; *MT-ND4* reverse, TAGCAGTTCTTGTGAGCTTTCTCGGT; 5′ end of *ND5*, *MT-ND5* forward, AACATGGCTTTCTCAACTTTTAAAGGATAAC; *MT-ND5* reverse, CGTTTGTGTATGATATGTTTGCGGTTTC; *ND6* and 3′ end of *ND5*, *MT-ND5* and *MT-ND6* forward, ACTTCAACCTCCCTCACCATTGG; *MT-ND5* and *MT-ND6* reverse, TCATTGGTGTTCTTGTAGTTGAAATACAAC.

Cell counting. For cell proliferation assays, cell counting was carried out by plating cells in triplicate in 24-well plates at 5,000 to 20,000 cells per well in 2 ml RPMI base media under the conditions described in each experiment (that is, varying glucose concentration or phenformin treatment). After 4 days, the entire contents of the well were resuspended and counted (suspension cells) or trypsinized, resuspended and counted (adherent cells) using a Beckman Z2 Coulter Counter with a size selection setting of 8 to 30 μm. The increase in cell number compared to the initially plated sample was calculated and all values were normalized to their control in 10 mM glucose unless otherwise indicated.

ATP-based measurements. ATP-based measurements for cell-proliferation assays were carried out by plating cells in replicates of five in 96-well plates at 500 to 1,000 cells per well in 200 μl RPMI base media under the conditions described in each experiment, and a separate group of five wells was also plated for each cell line with no treatment for an initial time point. After 5 h (untreated cells for initial time point) or after 3 days (with varying treatment conditions), 40 μl of Cell Titer Glo reagent (Promega) was added to each well, mixed briefly, and the luminescence read on a Luminometer (Molecular Devices). For wells with treatments causing an increase in luminescence, the fold change in luminescence relative to the initial luminescence was computed and this fold change for each condition was normalized to untreated wells (no effect = 1). For wells with treatments causing a decrease in luminescence, the fold decrease in luminescence relative to the initial luminescence was computed (no viable cells present = −1).

qPCR. RNA was isolated using the RNeasy Kit (Qiagen) according to the manufacturer's protocol. RNA was spectrophotometrically quantified and equal amounts were used for cDNA synthesis with the Superscript II RT Kit (Invitrogen). To isolate genomic and mitochondrial DNA we used the Blood and Tissue Kit (Qiagen). qPCR analysis of gene expression or copy number was performed on an ABI Real Time PCR System (Applied Biosystems) with the SYBR green Mastermix (Applied Biosystems).

All primers were designed using the Primer3 software and aligned to the human reference genomes using blast to verify their specificity. The primers used for GLUT3 and GLUT1 are as follows *GLUT1* forward and reverse, TCGTCGGCAT CCTCATCGCC and CCGGTTCTCCTCGTTGCGGT; *GLUT3* forward and reverse, TTGCTCTTCCCCTCCGCTGC and ACCGTGTGCCTGCCCTTCAA. Results were normalized to RPL0 levels.

Oxygen consumption. Oxygen consumption of intact or permeabilized cells was measured using an XF24 Extracellular Flux Analyzer (Seahorse Bioscience). For suspension cells, seahorse plates were coated with Cell TAK (BD, 0.02 mg ml^{-1} in 0.1 μM $NaHO_3$) for 20 min to increase adherence of suspension cells. Then 250,000 cells were attached to the plate by centrifugation at 1,000*g*, without brakes for 5 min. For adherent cells, 40,000 to 80,000 cells were plated the night before the experiments. RPMI 8226 (US biological no. 9011) was used as the assay media for all experiments with the indicated glucose concentrations in the presence of 2 mM glutamine without serum. For spare respiratory capacity measurements, increasing FCCP concentrations (0.1, 0.5 and 2 μM) were used in order to assess maximum OCR of each cell line. For basal oxygen consumption measurements, cell number or protein concentration was used for normalization.

Permeabilized cell measurements were performed as described previously[27]. In brief, cells were resuspended and plated (300,000 cells in 500 μl per well) in MAS-1 buffer (70 mM Sucrose, 220 mM Mannitol, 10 mM KH_2PO_4, 5 mM $MgCl_2$, 2 mM HEPES, 1 mM EGTA, 0.2% fatty-acid-free BSA, pH 7.2). Saponin (50 μg ml^{-1}), methyl pyruvate and malate (10 mM and 5 mM, respectively) were used for functional assessment of complex I, succinate (5 mM), rotenone (0.5 μM) and antimycin (1 μM) for functional assessment of complex II and III, TMPD and ascorbate (10 mM and 50 mM, respectively) for functional assessment of complex IV. 4 mM ADP was added to permeabilized cells to activate respiration in the mitochondria. We used the complex V inhibitor oligomycin (0.5 μM) to measure oxygen consumption in the absence of oxidative phosphorylation. All compounds were diluted in the assay buffer and injected into the wells sequentially as indicated for each experiment.

Mouse xenografts. Xenografts were initiated with 2- to 5-million cells per injection site implanted subcutaneously into the right and left flanks of 5- to 8-week-old male NOD.CB17 Scid/J mice (Jackson Laboratories). Once tumours were palpable in all animals (>50 mm^3 volume by caliper measurements), mice were assigned randomly into biguanide treated or untreated groups and caliper measurements were taken every 3 to 4 days until tumour burden approached the limits set by institutional guidelines. Tumour volume was assessed according to the formula: $0.5 \times W \times W \times L$ or $1.33 \times W/2 \times L/2 \times D/2$ for large tumours (W, width; L, length; D, depth). Phenformin was delivered in drinking water as described previously[15] at 1.7 mg ml^{-1} concentration with 5 mg ml^{-1} sucralose (Splenda), and metformin was delivered by daily intraperitoneal injection (300 mg kg^{-1}). All experiments involving mice were carried out with approval from the Committee for Animal Care at MIT and under supervision of the Department of Comparative Medicine at MIT.

Mitochondrial DNA copy number and mass. For relative mitochondrial mass measurements, 2×10^5 cells were incubated directly with 50 nM Mitotracker Green FM (Invitrogen M7514) in RPMI for 40 min at 37 °C. Cells were then centrifuged at 1,000*g* for 5 min at 4 °C and the overlying media removed. Cells were kept on ice, washed once with ice-cold PBS, and resuspended in ice-cold PBS with 7-AAD (Invitrogen A1310) for FACS (fluorescence-activated cell sorting) analysis of live cells. The mean Mitotracker Green fluorescence intensity was used as a measure of relative mitochondrial mass.

For copy number, total DNA was isolated using the QIAamp DNA Minikit and qPCR was used to estimate relative differences in mtDNA copy number between different cell lines. *Alu* repeat elements were used as controls. Primers used are, *ND1* forward and reverse, CCCTAAAACCCGCCACATCT and GAGCGATGG TGAGAGCTAAGGT; *ND2* forward and reverse, TGTTGGTTATACCCTTCC CGTACTA and CCTGCAAAGATGGTAGAGTAGATGA; *Alu* forward and reverse, CTTGCAGTGAGCCGAGATT and GAGACGGAGTCTCGCTCTGTC.

Selection of cells in phenformin. Cal-62 cells were selected at a concentration of phenformin that permitted half-maximal growth compared to the unselected line (approximately 5 μM for 2 weeks, 10 μM for 1.5 weeks, 15 μM for 1.5 weeks, and 20 μM for 1 week). Cells were split 1:10 when nearing confluence. After selection, cells were removed from phenformin for at least 3 days before starting proliferation assays. The ratio of wild-type to mutant mtDNA was calculated by summing the 11 Sanger sequencing peak height measurements per nucleotide position for both the wild-type and mutant allele allowing for the percentage of mutant mtDNA alleles to be calculated. These values were averaged over three nucleotide positions for which the base in the wild type and mutant sequence differs.

Cell competition assay for KMS-26 cells with control and GLUT3 vector. KMS-26 cells with vector control and GLUT3 overexpression were mixed in equal amounts and an initial mixed sample was collected. Mixed cells were then cultured in different glucose concentrations *in vitro* and additionally injected subcutaneously to NOD-SCID mice. After 2.5 weeks, genomic DNA was isolated from initial sample, cells cultured in different glucose concentrations *in vitro*, and tumours grown in mice. Using a 5′ common primer targeting the vector (AGTAGACGG CATCGCAGCTTGGATA) and 3′ primers targeting the vector (GGCGGAATT TACGTAGCGGCC) or GLUT3 (GAGCCGATTGTAGCAACTGTGATGG), the abundance of the integrated viruses were determined by qPCR and the relative abundance of KMS-26 vector and KMS-26 GLUT3 cells inferred.

Statistics and animal-model statements. All experiments reported in Figs 1–4 were repeated at least three times in the laboratory, except Fig. 4f, g, which was performed once. *t*-tests were heteroscedastic to allow for unequal variance and distributions assumed to follow a Student's *t* distribution, and these assumptions are not contradicted by the data. No samples or animals were excluded from analysis, and sample size estimates were not used. Animals were randomly assigned into a treatment group with the constraint that the starting tumour burden in the treatment and control groups were similar. Studies were not conducted blind.

25. Possemato, R. *et al.* Functional genomics reveal that the serine synthesis pathway is essential in breast cancer. *Nature* **476,** 346–350 (2011).
26. Birsoy, K. *et al.* MCT1-mediated transport of a toxic molecule is an effective strategy for targeting glycolytic tumors. *Nature Genet.* **45,** 104–108 (2013).
27. Clerc, P. & Polster, B. M. Investigation of mitochondrial dysfunction by sequential microplate-based respiration measurements from intact and permeabilized neurons. *PLoS ONE* **7,** e34465 (2012).

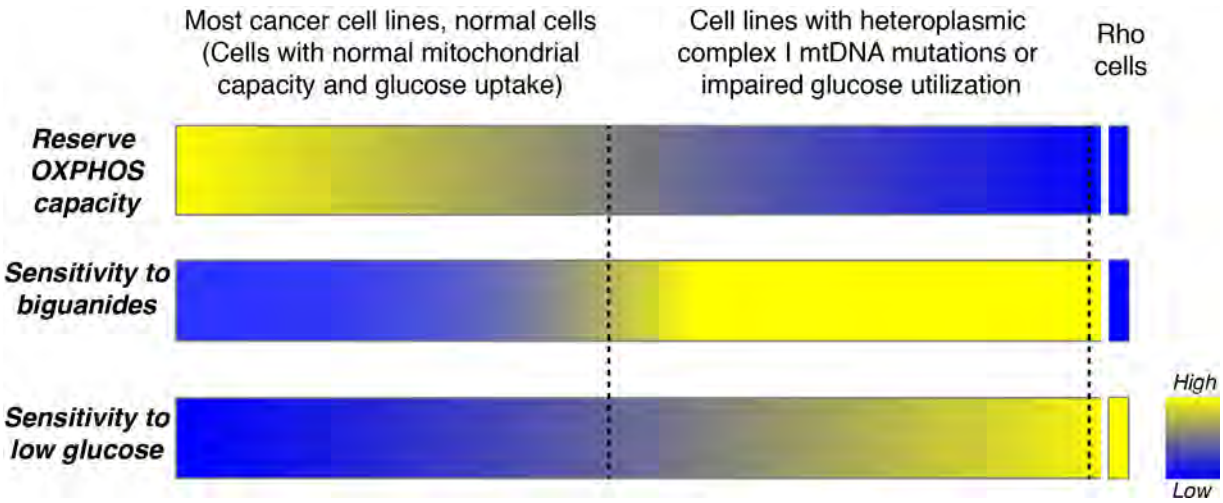

Extended Data Figure 1 | Model of the metabolic determinants of sensitivity to low glucose and biguanides. This diagram outlines the interplay between reserve oxidative phosphorylation (OXPHOS) capacity, sensitivity to biguanides, and sensitivity to culture in low glucose. Most cancer cell lines and normal cells tested exhibited an ability to respond to glucose limitation by upregulating OXPHOS, rendering them less sensitive to biguanides and low-glucose conditions. In contrast, cell lines harbouring mutations in mtDNA-encoded complex I subunits or exhibiting impaired glucose utilization have a limited reserve OXPHOS capacity and are therefore unable to properly respond to biguanides and low glucose, rendering them sensitive to these perturbations. At the extreme, cells artificially engineered to have no OXPHOS (Rho cells) exhibit extreme low glucose sensitivity, but resistance to further inhibition of OXPHOS. Thus, mtDNA mutant cancer cells exist at an intermediate state of OXPHOS functionality that renders them sensitive to treatment with biguanides *in vitro* and *in vivo*. Similarly, cell lines with impaired glucose utilization exhibit biguanide sensitivity specifically under the low glucose conditions seen in the tumour microenvironment.

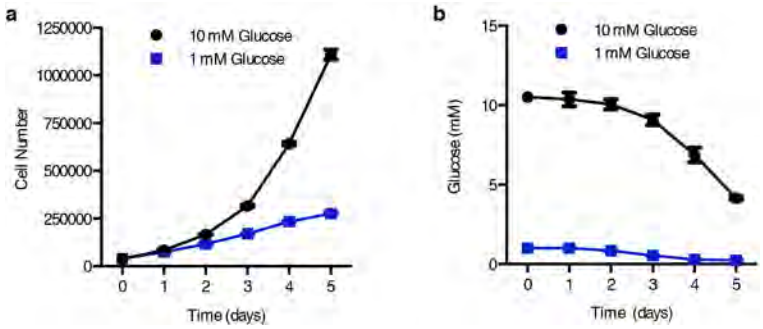

Extended Data Figure 2 | Proliferation and media glucose levels in standard culture conditions. **a**, Jurkat cell proliferation under 10 mM (black) versus 1 mM (blue) glucose in standard culture conditions. **b**, Media glucose concentrations over time from cultures in **a**. Error bars are s.e.m., $n = 3$. Replicates are biological, means reported. *$P < 0.05$ by two-sided student's *t*-test.

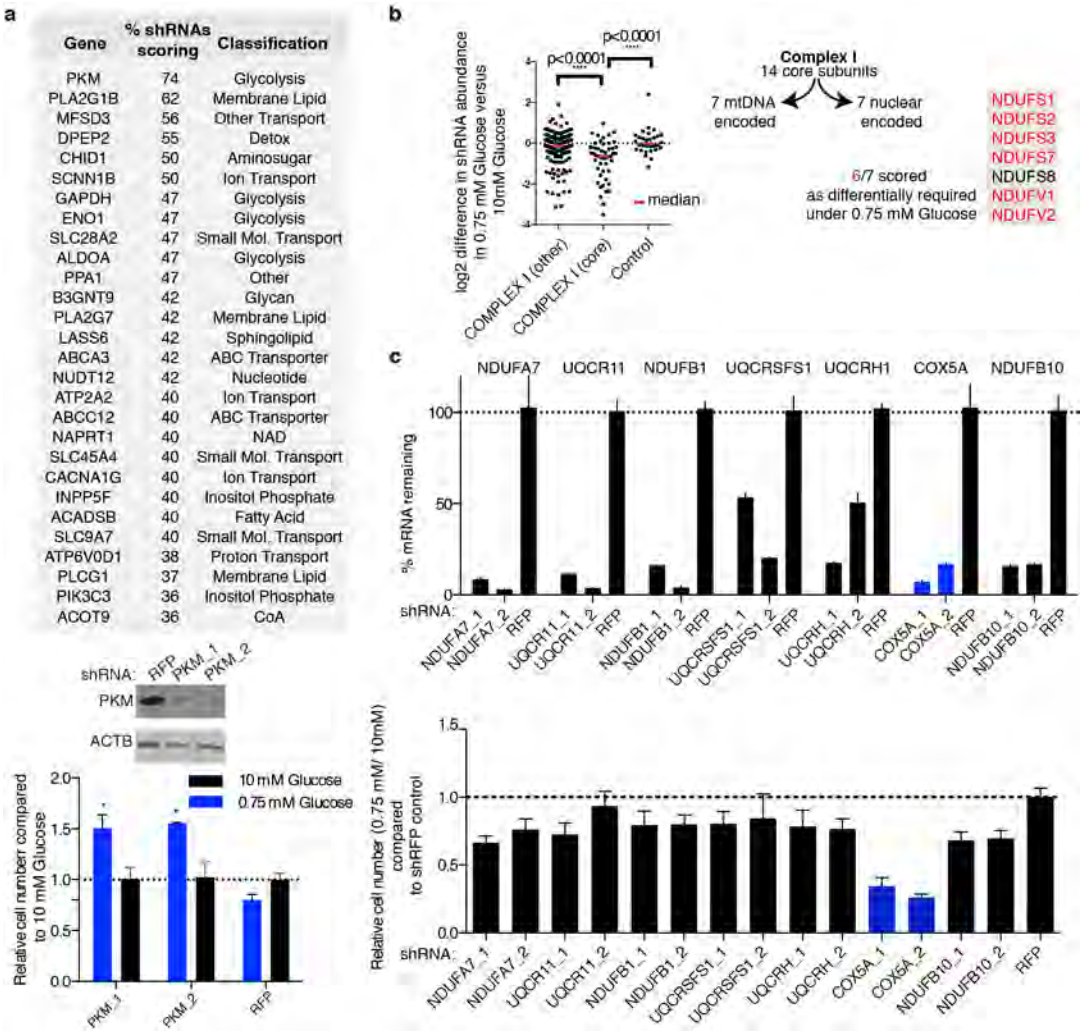

Gene	% shRNAs scoring	Classification
PKM	74	Glycolysis
PLA2G1B	62	Membrane Lipid
MFSD3	56	Other Transport
DPEP2	55	Detox
CHID1	50	Aminosugar
SCNN1B	50	Ion Transport
GAPDH	47	Glycolysis
ENO1	47	Glycolysis
SLC28A2	47	Small Mol. Transport
ALDOA	47	Glycolysis
PPA1	47	Other
B3GNT9	42	Glycan
PLA2G7	42	Membrane Lipid
LASS6	42	Sphingolipid
ABCA3	42	ABC Transporter
NUDT12	42	Nucleotide
ATP2A2	40	Ion Transport
ABCC12	40	ABC Transporter
NAPRT1	40	NAD
SLC45A4	40	Small Mol. Transport
CACNA1G	40	Ion Transport
INPP5F	40	Inositol Phosphate
ACADSB	40	Fatty Acid
SLC9A7	40	Small Mol. Transport
ATP6V0D1	38	Proton Transport
PLCG1	37	Membrane Lipid
PIK3C3	36	Inositol Phosphate
ACOT9	36	CoA

Extended Data Figure 3 | Additional data supporting the RNAi screen. **a**, Genes scoring as preferentially required for growth in 10 mM glucose compared to 0.75 mM glucose (top). shRNAs scores (given in per cent) and pathway classifications are indicated. Immunoblot analyses depict suppression of PKM by shRNAs (PKM1, PKM2) compared to control (RFP). Proliferation of cells in 0.75 mM (blue) relative to 10 mM glucose (black) harbouring shRNAs targeting PKM or control is also shown (PKM1). *$P < 0.05$ relative to RFP 0.75 mM glucose. **b**, Nuclear-encoded core complex I genes are shown in the grey box, with those that scored as differentially required under 0.75 mM glucose in red. The dot plot reports the degree of differential requirement for growth in 0.75 mM glucose (as the $\log_2$ difference in shRNA abundance in 0.75 mM glucose versus 10 mM glucose) of individual shRNAs targeting non-core complex I genes, core complex I genes, or non-targeting controls. Red bar, population median. **c**, Top, mRNA levels of the non-scoring OXPHOS genes (black) and the scoring OXPHOS gene (blue) indicated upon suppression, with the shRNAs indicated as measured by qPCR, relative to a non-targeting shRNA (RFP). Bottom, cell number from 7-day proliferation assay of cells in 0.75 mM glucose relative to 10 mM glucose (not shown) harbouring the indicated shRNAs. shRFP control normalized to 1. Error bars are s.e.m., $n = 3$. Replicates are biological, means reported. *$P < 0.05$ by two-sided student's t-test.

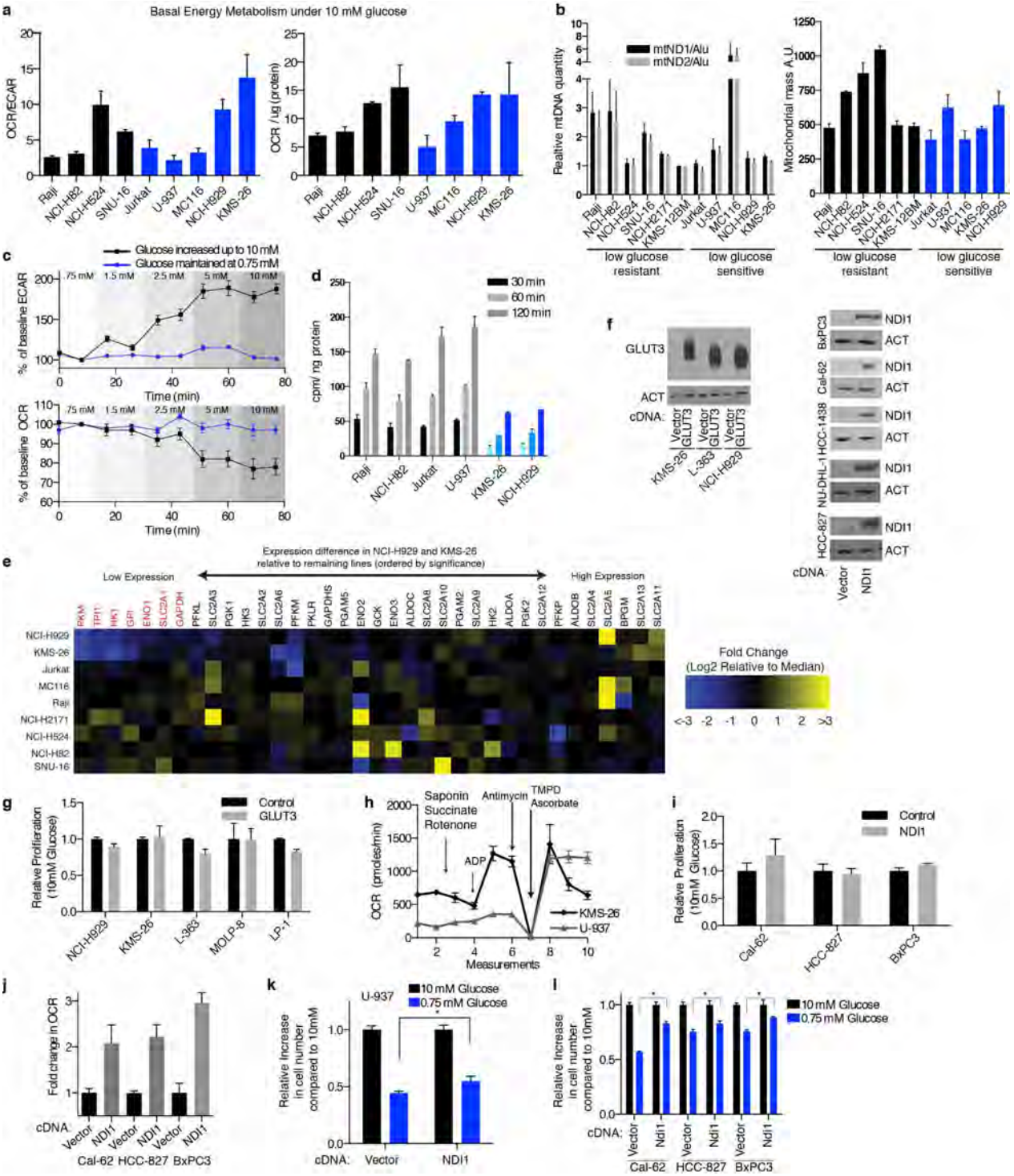

Extended Data Figure 4 | Additional data characterizing mitochondrial dysfunction and impaired glucose utilization in cancer cell lines. **a**, Ratio of oxygen consumption rate (OCR) to extracellular acidification rate (ECAR) (left) or OCR normalized to protein content (right) for glucose-limitation-resistant (black) or glucose-limitation-sensitive (blue) cell lines. **b**, Left, mtDNA content for indicated cell lines by qPCR using primers targeting ND1 (black) or ND2 (grey) normalized to gDNA repetitive element (Alu) relative to KMS-12BM. Right, mitochondrial mass measured by fluorescence intensity of Mitotracker Green dye for indicated cell lines. **c**, Per cent change from baseline (second measurement) of ECAR or OCR in Jurkat cells in conditions in which glucose concentration was maintained at 0.75 mM (blue) or increased to indicated concentrations (black). **d**, Uptake of 3H-labelled 2-DG (counts per min per ng protein) in 0.75 mM glucose at indicated time points in GLUT3-high (grey) or GLUT3-low (blue) cell lines. **e**, Heatmap of gene expression values for genes indicated at top and cell lines (left). Genes organized by *P* value with lowest expressed genes in NCI-H929 and KMS-26 to the left, those with significantly lower expression are in red. Expression values reported as $\log_2$-transformed fold difference from the median (scale colour bar shown to the right). **f**, Immunoblot analyses for GLUT3 and NDI1 expression in indicated cell lines (β-actin loading control). **g**, **i**, Proliferation of cell number in cells overexpressing GLUT3 or NDI1 relative to control vector (4 days). **h**, OCR of permeabilized cells indicated upon addition of indicated metabolic toxins and substrates. **j**, Fold change in OCR in indicated cells expressing NDI1 relative to control vector. **k**, **l**, Proliferation for 4 days of control (Vector) or NDI1 expressing cell lines indicated (NDI1) under 10 mM (black) and 0.75 mM glucose (blue). Error bars are s.e.m. $n = 4$ for **a**–**c**, **h**, **j**; $n = 3$ for **d**, **g**, **i**, **k**, **l**. Replicates are biological, means reported. $^*P < 0.05$ by two-sided student's *t*-test.

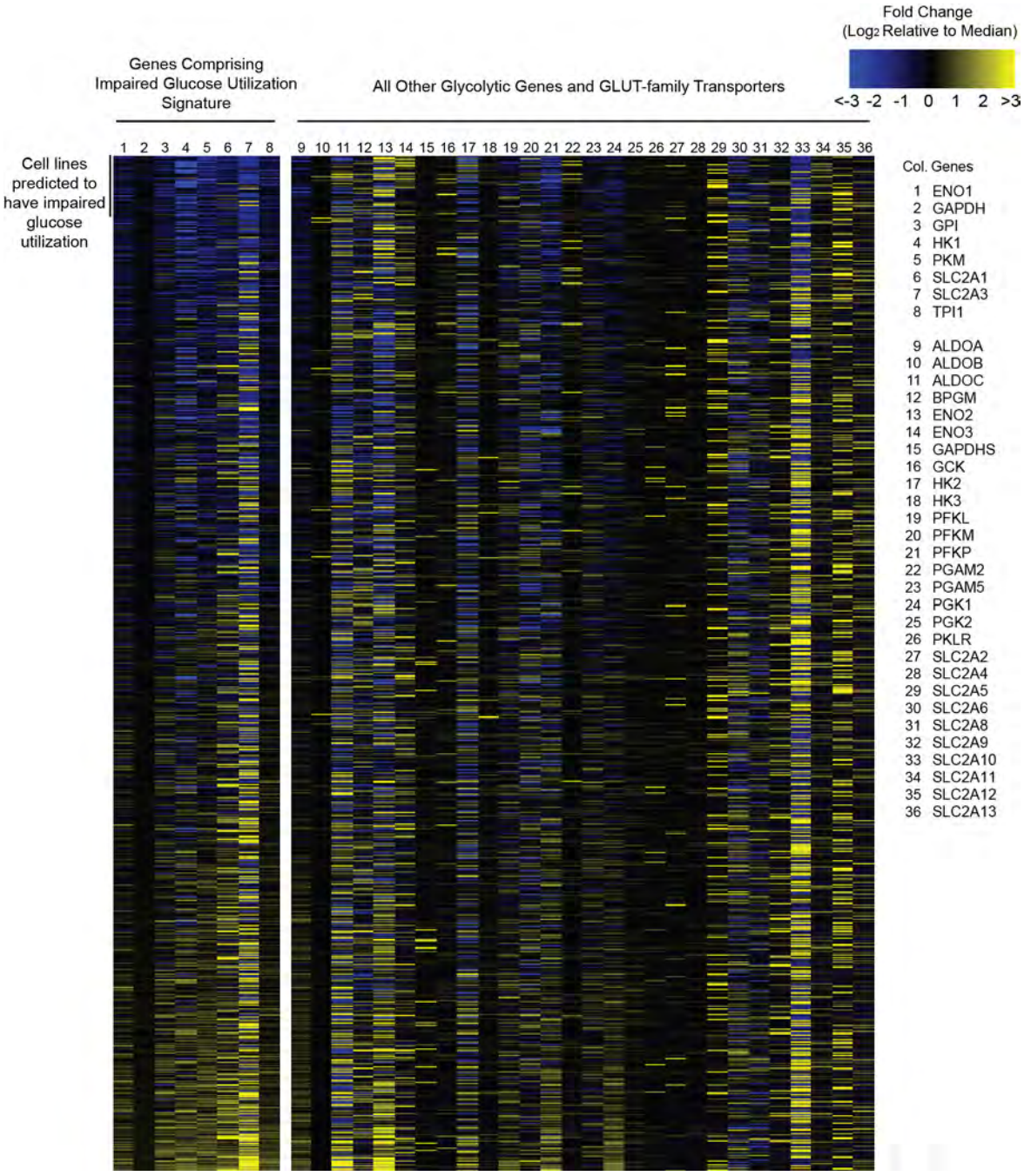

Extended Data Figure 5 | Gene expression signature for identifying cell lines with impaired glucose utilization. Heatmap of gene expression values for the genes indicated on the right for the cell lines in the CCLE set. Gene expression values are reported as the difference from the median across the entire sample set according to the scale colour bar to the top right. Genes 1–8 comprised the gene expression signature used to identify samples with impaired glucose utilization. Samples are sorted based upon this signature, with those predicted to exhibit impaired glucose utilization at the top. The order of samples and all values are reported in Supplementary Table 4.

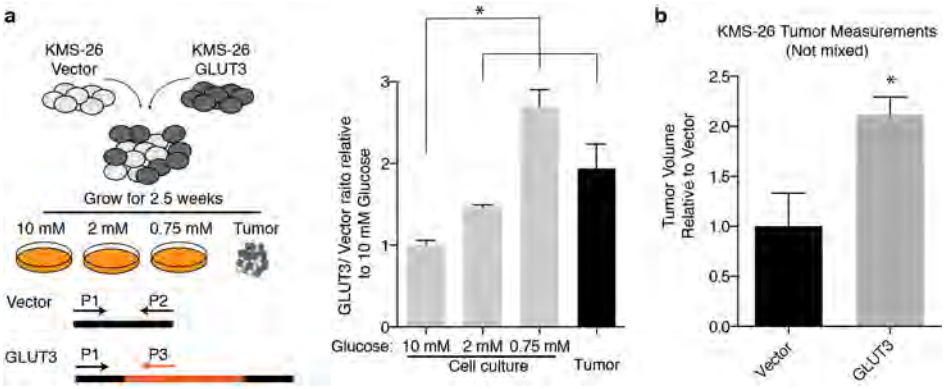

Extended Data Figure 6 | GLUT3 overexpression increases tumour xenograft growth and cell proliferation in low-glucose media. a, KMS-26 cell lines infected with GLUT3-overexpressing vector or infected with control vector were mixed in equal proportions and cultured under different glucose concentrations. In addition, these mixed cell lines were injected into NOD/SCID mice subcutaneously. After 2.5 weeks, genomic DNA was isolated from tumours as well as cells grown *in vitro* under the indicated glucose concentrations. Using qPCR, relative abundance of control vector and GLUT3 vector were determined and plotted relative to 10 mM glucose in culture ($n = 9$). **b**, Average volume of unmixed tumour xenografts from KMS-26 cell lines infected with GLUT3-overexpressing vector relative to control vector (2.5 weeks) ($n = 6$). Replicates are biological, means reported. *$P < 0.05$ by two-sided student's *t*-test.

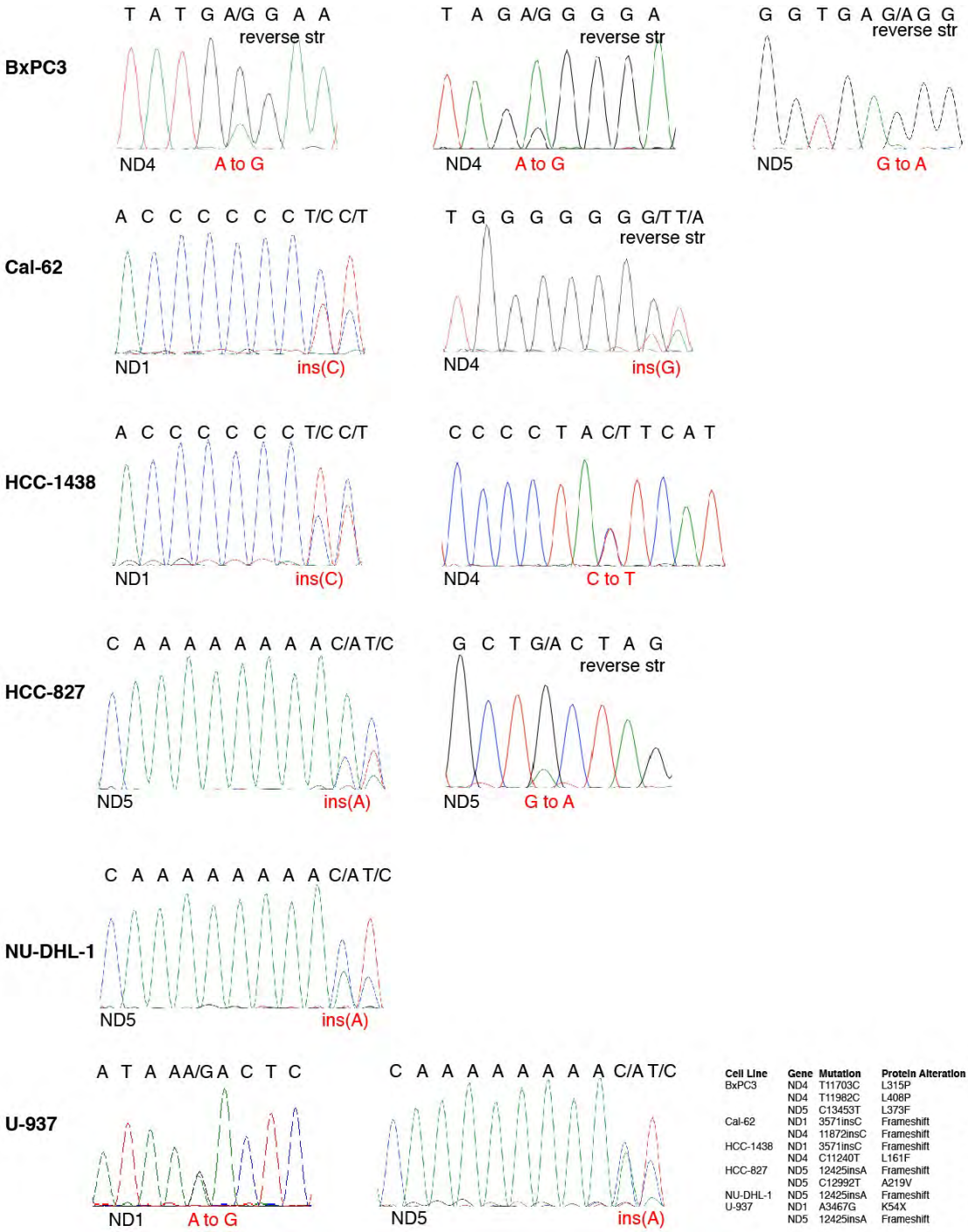

Cell Line	Gene	Mutation	Protein Alteration	Heteroplasmy
BxPC3	ND4	T11703C	L315P	80% mutant
	ND4	T11982C	L408P	25%
	ND5	C13453T	L373F	15%
Cal-62	ND1	3571insC	Frameshift	70%
	ND4	11872insC	Frameshift	80%
HCC-1438	ND1	3571insC	Frameshift	45%
	ND4	C11240T	L161F	50%
HCC-827	ND5	12425insA	Frameshift	80%
	ND5	C12992T	A219V	20%
NU-DHL-1	ND5	12425insA	Frameshift	40%
U-937	ND1	A3467G	K54X	50%
	ND5	12425insA	Frameshift	50%

Extended Data Figure 7 | Sanger sequencing traces validating mtDNA mutations. The table summarizing mtDNA mutations in complex I subunits from Fig. 3j is reproduced (bottom right). Traces for each cell line (left) are shown in the order indicated by the table. In cases in which the sequence shown is in the reverse orientation to the revised Cambridge Reference Sequence, these are indicated by 'reverse str'. For each trace, the gene sequenced is at the bottom left, the DNA sequence is at the top, and the nucleotide alteration is in red text.

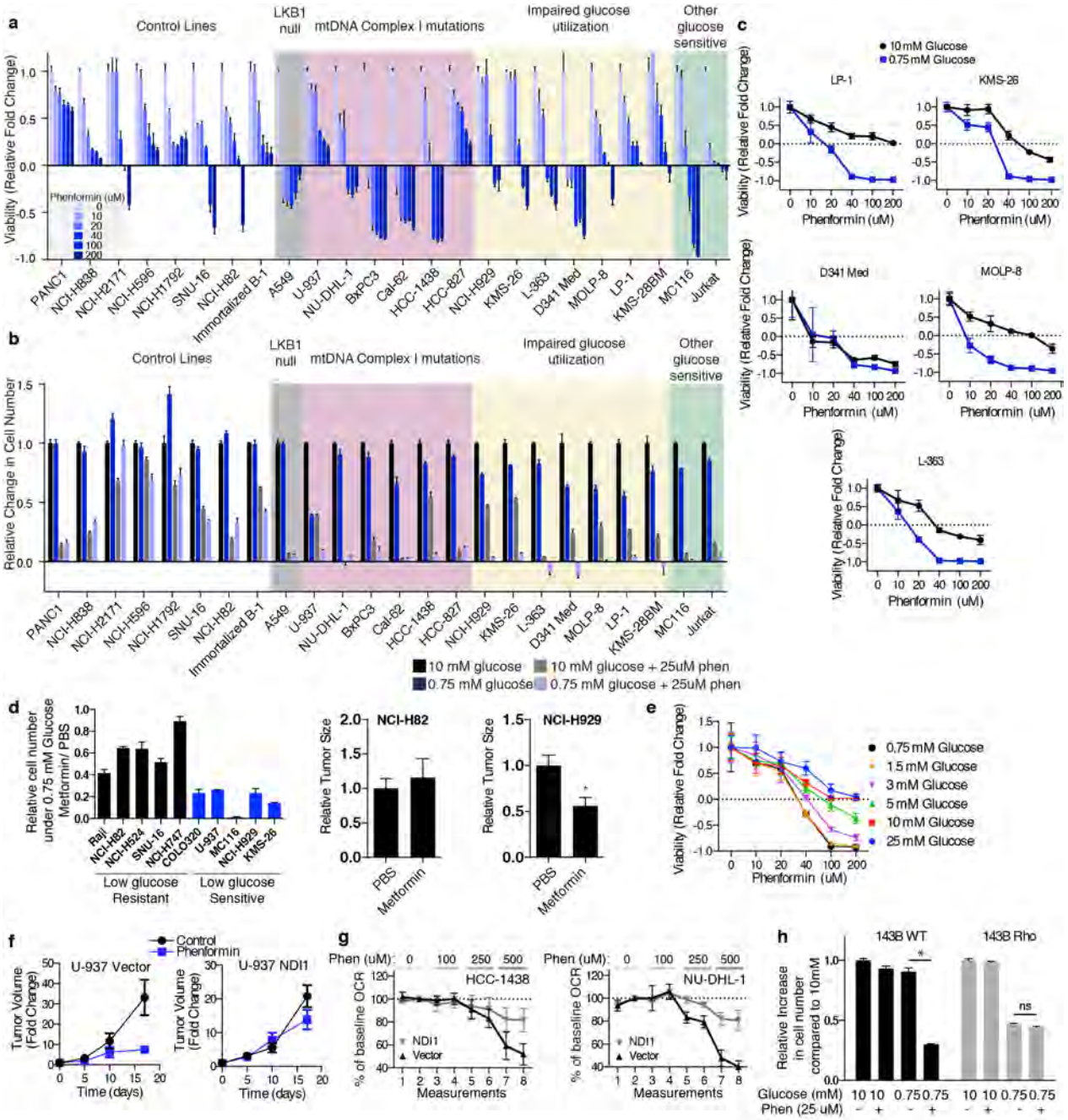

Extended Data Figure 8 | Additional data supporting the hypersensitivity of cell lines with the identified biomarkers to biguanides. **a**, **b**, Viability (**a**, 10 mM glucose) or relative change in cell number (**b**, 4 days, glucose concentration indicated in key) of indicated cell lines at phenformin concentrations indicated. Viability measured by ATP levels on day 3 at phenformin concentrations indicated by the black–blue scale, compared to ATP levels on day 0. Value of 1 indicates fully viable cells (untreated). Value of 0 indicates no change in ATP level compared to day 0 (cytostatic). Negative values indicate decrease in ATP levels (−1 indicates no ATP). **c**, Viability as in **a** of indicated cell lines under 0.75 mM and 10 mM glucose at indicated phenformin concentrations. **d**, Left, relative change in cell number in 0.75 mM glucose, 2 mM metformin relative to untreated in glucose limitation resistant (black) and sensitive (blue) cell lines. Right, relative size of tumour xenografts derived from the indicated cell lines in mice injected with PBS or metformin (intraperitoneal, 300 mg kg^{-1} day^{-1}). **e**, Viability as in **a** of NCI-H929 cells at the indicated concentrations of phenformin and glucose. **f**, Relative size of indicated cell line xenografts in mice treated with PBS or phenformin (1.7 mg ml^{-1} in drinking water). **g**, Per cent change in OCR of control (Vector) or NDI1-expressing lines (NDI1) relative to the second basal measurement and at indicated phenformin concentrations. **h**, Proliferation of 143B wild-type or 143B rho (no mtDNA) cell lines under 0.75 mM or 10 mM glucose with or without phenformin treatment. Error bars are s.e.m. $n = 4$ for **a**, **c**, **e**, **g**; $n = 3$ for **b**, **d**, **h** (left); $n = 5$ for **d** (right), **f**. Replicates are biological, means reported. *$P < 0.05$ by two-sided student's *t*-test.

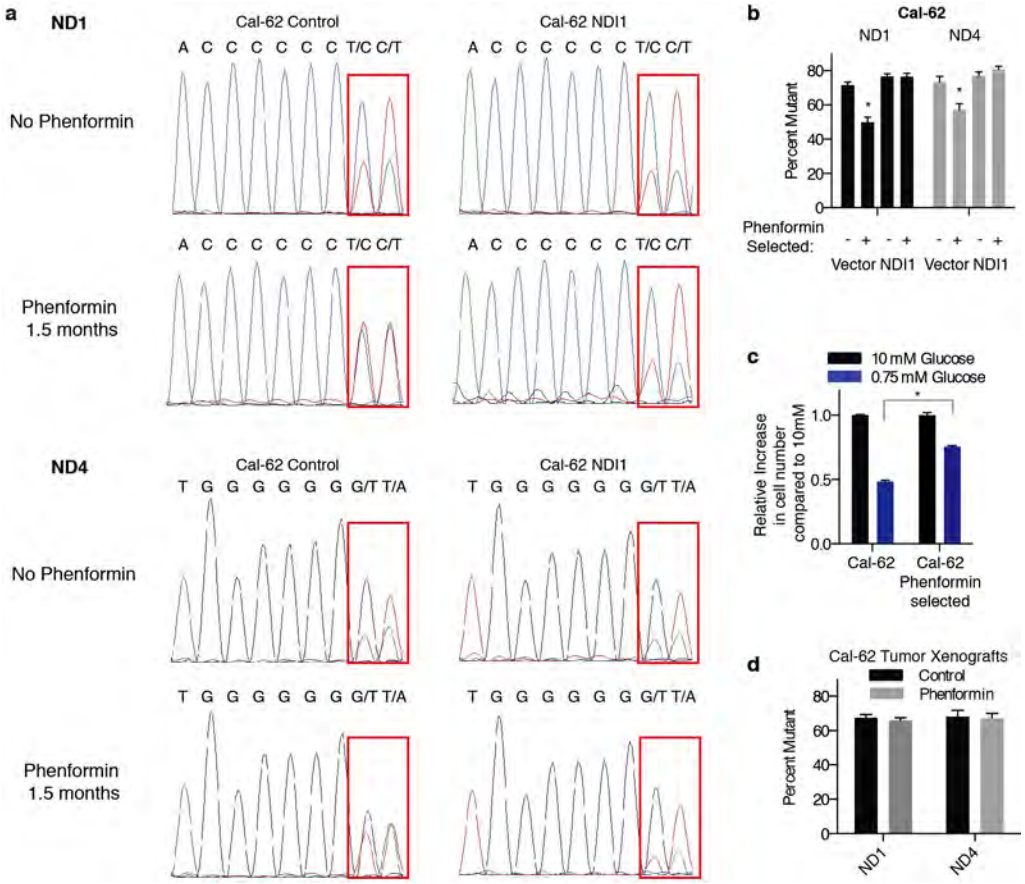

Extended Data Figure 9 | Long-term treatment of mtDNA mutant cells with phenformin. **a**, Sanger sequencing traces of mtDNA-encoded *ND1* and *ND4* genes from Cal-62 cells expressing NDI1 or control vector cultured under 5 to 20 μM phenformin or no phenformin for 1.5 months. Regions containing mutant sequence are indicated by the red box. **b**, Heteroplasmy levels for mutation in *ND1* or *ND4* were assessed by measuring the relative areas under the curve from Sanger-sequencing and plotted. **c**, Cal-62 cell lines cultured with or without phenformin for 1.5 months assessed for their ability to proliferate in 0.75 mM glucose (blue) relative to 10 mM glucose (black). The proliferation assay was for 4 days in the absence of phenformin. **d**, Heteroplasmy levels of *ND1* and *ND4* as in **b** of Cal-62 tumour xenografts in mice treated with or without phenformin for 28 days. Error bars are s.e.m., $n = 3$. Replicates are biological (**c**) or technical (**b**, **d**), means reported. $^*P < 0.05$ by two-sided student's *t*-test.

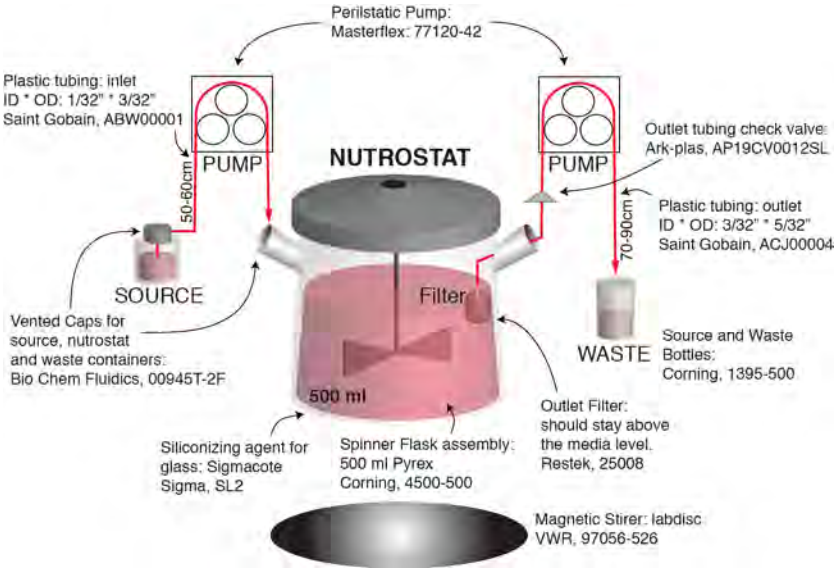

Extended Data Figure 10 | Schematic of Nutrostat setup. Part numbers, sizes and dimensions for the Nutrostat assembly are indicated (see Methods for additional details).